NACA RM L50I27

NACA

RESEARCH MEMORANDUM

THE LONGITUDINAL STABILITY, CONTROL EFFECTIVENESS, AND CONTROL HINGE-MOMENT CHARACTERISTICS OBTAINED FROM A FLIGHT INVESTIGATION OF A CANARD MISSILE CONFIGURATION AT TRANSONIC AND SUPERSONIC SPEEDS

By Roy J. Niewald and Martin T. Moul

Langley Aeronautical Laboratory
Langley Air Force Base, Va.

NATIONAL ADVISORY COMMITTEE
FOR AERONAUTICS

WASHINGTON

November 24, 1950
Declassified September 15, 1955

NACA RM L50I27

NATIONAL ADVISORY COMMITTEE FOR AERONAUTICS

RESEARCH MEMORANDUM

THE LONGITUDINAL STABILITY, CONTROL EFFECTIVENESS, AND CONTROL HINGE-MOMENT CHARACTERISTICS OBTAINED FROM A FLIGHT INVESTIGATION OF A CANARD MISSILE CONFIGURATION AT TRANSONIC AND SUPERSONIC SPEEDS

By Roy J. Niewald and Martin T. Moul

SUMMARY

A flight investigation has been made to determine the longitudinal stability and control characteristics of a 60° delta wing canard missile configuration. The results include the longitudinal stability derivatives, control effectiveness, drag characteristics, and control-surface hinge-moment characteristics for a Mach number range of 0.7 to 1.45.

The longitudinal stability derivatives showed no unusual trends and a gradual variation with Mach number at transonic and supersonic velocities and appeared to be linear functions of angle of attack within the accuracy of the data and for the small angle-of-attack range obtained in flight. The aerodynamic-center position showed a rearward shift of 12 percent of the mean aerodynamic chord between Mach numbers of 0.9 and 1.25.

Control pitching effectiveness was maintained throughout the Mach number range, although lift produced by control deflection was slightly positive at subsonic speeds and slightly negative at supersonic speeds.

Hinge moments were very low at all Mach numbers tested, especially at supersonic speeds; therefore, excellent aerodynamic balancing characteristics can be obtained with all-movable delta control surfaces.

The variation of minimum drag coefficient with Mach number showed a sudden increase at a Mach number of 0.85 to a maximum value at $M = 1.05$. The maximum lift-drag ratio at supersonic velocities was about 3.7.

INTRODUCTION

As part of the general research program on guided missiles, the Langley Pilotless Aircraft Research Division has been conducting a series of flight tests to determine the stability and control characteristics of a canard missile configuration. The aerodynamic parameters are necessary for the analysis and design of various automatic stabilization systems and will also provide useful aerodynamic design data for estimating the stability and control characteristics of similar configurations.

The longitudinal stability, control, hinge-moment, and drag characteristics obtained from the flight test of a 60° delta wing canard missile configuration at the Langley Pilotless Aircraft Research Station at Wallops Island, Va. are presented for a Mach number range of 0.7 to 1.45. The results were obtained through the use of a model utilizing a programmed control system.

The rolling stability and control derivatives and aileron hinge-moment characteristics of this configuration using wing-tip ailerons have been reported in reference 1. Results of the flight test of a model incorporating a roll-stabilization system were presented in reference 2.

SYMBOLS

c	wing chord, feet
$\bar{c}$	wing mean aerodynamic chord (1.49 ft)
S_w	total wing area in one plane (2.89 sq ft)
$\bar{c}_e$	canard control-surface mean aerodynamic chord (0.387 ft)
S_e	canard control-surface exposed area (0.192 sq ft)
t	wing thickness, inches; or time, seconds
W	weight (115.4 lb)
I_Y	moment of inertia about Y-axis (20.0 slug-ft^2)
ρ	mass density of air, slugs per cubic foot
μ	coefficient of viscosity, slugs per foot-seconds
V	velocity of model, feet per second

V_c speed of sound in air, feet per second

M Mach number (V/V_c)

R Reynolds number $(\rho V\bar{c}/\mu)$

q dynamic pressure, pounds per square foot $\left(\frac{1}{2}\rho V^2\right)$; or pitching velocity, degrees per second

g acceleration due to gravity, feet per second per second

α angle of attack, degrees

$\dot{\alpha} = \frac{d\alpha}{dt}$, degrees per second

δ_e canard control deflection, degrees

a_n/g normal accelerometer reading, g units

a_l/g longitudinal accelerometer reading, deceleration positive, g units

H hinge moment, foot-pounds

ac aerodynamic center

C_L lift coefficient $\left(\left(\frac{a_n}{g}\cos\alpha - \frac{a_l}{g}\sin\alpha\right)\frac{W}{qS_w}\right)$

C_D drag coefficient $\left(\left(\frac{a_l}{g}\cos\alpha + \frac{a_n}{g}\sin\alpha\right)\frac{W}{qS_w}\right)$

C_m pitching-moment coefficient $\left(\frac{\text{Pitching moment}}{qS_w\bar{c}}\right)$

C_h hinge-moment coefficient $\left(\frac{H}{qS_e\bar{c}_e}\right)$

$C_{L_{trim}}$ trim lift coefficient

α_{trim} trim angle of attack, degrees

$C_{L_\alpha} = \frac{\partial C_L}{\partial \alpha}$, per degree

$C_{m_\alpha} = \frac{\partial C_m}{\partial \alpha}$, per degree

$C_{m_q} = \frac{\partial C_m}{\partial \frac{qc}{2V}}$, per degree

$C_{m_{\dot{\alpha}}} = \frac{\partial C_m}{\partial \frac{\dot{\alpha} c}{2V}}$, per degree

$C_{L_{\delta_e}} = \frac{\partial C_L}{\partial \delta_e}$, per degree

$C_{m_{\delta_e}} = \frac{\partial C_m}{\partial \delta_e}$, per degree

$C_{h_\alpha} = \frac{\partial C_h}{\partial \alpha}$, per degree

$C_{h_{\delta_e}} = \frac{\partial C_h}{\partial \delta_e}$, per degree

C_{h_0} hinge-moment coefficient at 0° angle of attack and 0° control deflection

$C_{D_{min}}$ minimum drag coefficient

$(L/D)_{max}$ maximum lift-drag ratio

P period, seconds

ω_{n_d} damped natural frequency, radians per second $(2\pi/P)$

b exponential damping coefficient in e^{-bt}, per second

$T_{1/2}$ time required for oscillations to damp to one-half amplitude, seconds $(0.693/b)$

MODEL DESCRIPTION

Sixty-degree delta wings and canard control surfaces were mounted on a cylindrical body of fineness ratio 16.3 with ogival nose and tail sections. The solid duralumin wings were fixed on the all-metal airframe in a cruciform fin arrangement with solid-steel control surfaces pivoted about a point on the body in line with and forward of the wings. A sketch of the model is shown in figure 1. Wing and control-surface details are shown in figure 2.

The wings and canard control surfaces had modified double-wedge airfoil sections with constant thicknesses corresponding to a thickness ratio of 3 percent at the wing-body juncture and 3 percent at the control-surface root chord.

The canard control surfaces were pulsed by a hydraulic servosystem in a square-wave motion from 5° to -5°. The control surfaces were actuated by a hydraulic piston which was supplied from an accumulator and programmed by a motor-driven valve.

A hinge-moment balance was also incorporated in the linkage system in order to measure hinge moments about a hinge line located at 64 percent of the root chord of the control surface.

The physical characteristics of the model are given in the following table:

Wing:	
S_w, square feet	2.89
M.A.C., feet	1.49
t/c at wing-body juncture	0.03
Canard control sufaces:	
S_e, square feet	0.192
M.A.C., feet	0.387
t/c at root chord	0.03
Weight, pounds	115.4
I_Y, slug-feet^2	20.00

INSTRUMENTATION

The model was equipped with an NACA six-channel telemeter which transmitted a continuous record of the normal and longitudinal accelerations, angle of attack, control deflection, control hinge moment, and intermittent total and calibrated static pressures. A free-floating vane mounted on a sting attached to the nose of the body was used for measuring angle of attack. Total pressure was obtained from a total-head tube extended below the fuselage.

The trajectory of the model was determined through the use of a radar tracking unit. The velocity of the model was measured by a CW Doppler velocimeter. Radiosonde data were used to obtain temperature and atmospheric pressure throughout the altitude range traversed by the model.

APPARATUS AND TECHNIQUE

The model contained no sustainer rocket motor but was boosted to supersonic velocities by means of a solid propellant rocket motor of 6,000-pound thrust and 3-second duration. Data were continuously recorded as the model coasted through the Mach number range after separation from the booster. Photographs of the model and the model-booster combination before launching are presented as figure 3.

The longitudinal stability and control derivatives were obtained by measuring the missile response to the step inputs of the canard control surfaces. The method of analysis used in the reduction of the data is given in the appendix.

ACCURACY

The accuracy of the various aerodynamic parameters determined from the flight records depended on the accuracy of measuring individual components such as dynamic pressure, angle of attack, and normal acceleration. Since the stability and control derivatives define the missile motion in flight, the accuracy of the analysis technique was indicated by comparing the measured missile response with the response calculated by using the derivatives. The calculated and measured angle-of-attack and normal acceleration responses are shown at a Mach number of 1.35 in figure 4. Good agreement was obtained between the measured and calculated response curves, this agreement indicating the validity of the equations of motion used in determining the derivatives and the accuracy of the

stability and control derivatives in determining the measured motions. The maximum difference between measured and calculated normal acceleration is about 0.8g or about 5 percent of the maximum acceleration obtained during the pulse cycle. The maximum difference between measured and calculated angle of attack is about 0.8° or 8 percent of the maximum angle of attack obtained during the pulse cycle.

The aerodynamic coefficients are subjected to possible errors in the telemeter and Doppler radar. Velocity is measured with an accuracy of approximately 1 percent and the error in dynamic pressure is then 2 percent, the error being proportional to the square of the velocity. The accuracy of any telemetered quantity is within 2 percent of the total calibrated instrument range. The resulting possible errors in the stability derivatives, drag and hinge-moment coefficients are tabulated at two Mach numbers as follows:

M	Percent of given value						
	C_{L_α}	C_{m_α}	$C_{L_{\delta_e}}$	$C_{m_{\delta_e}}$	$C_{m_q} + C_{m_{\dot{\alpha}}}$	C_h	C_D
0.80	3	4	40	6	16	5	8
1.40	2	4	40	6	10	10	4

The accuracy of $C_{L_{\delta_e}}$ is poor because, for the configuration tested, the magnitude of $C_{L_{\delta_e}}$ is approximately 4 percent that of C_{L_α}.

DISCUSSION OF THE RESULTS

The Reynolds number variation with Mach number for the flight-test conditions is shown in figure 5. Reynolds number was based on the wing mean aerodynamic chord. The scale of the flight tests is indicated by a range in Reynolds numbers of 6 to 15 million.

A typical section of the time histories obtained in flight of this model is shown in figure 6. The angle of attack, normal acceleration, and hinge-moment variations show the typical damped oscillations as the missile responded to the step control input. The longitudinal deceleration of the model is indicated by a Mach number decrease from $M = 1.38$ to $M = 1.21$ during a complete pulse cycle. All stability and control derivatives presented are partial derivatives based on total wing area in one plane and are referred to the wing mean aerodynamic chord. Hinge-moment derivatives are based on the control-surface exposed area and are referred to the control-surface mean aerodynamic chord.

Longitudinal stability derivatives.- The lift-curve slope C_{L_α} was obtained by measuring the slope of lift coefficient plotted against angle of attack. Lift coefficients were determined from the normal and longitudinal accelerations. The angle of attack measured at the nose of the model was corrected for flight-path curvature and pitching velocity to determine the angle of attack at the model center of gravity (reference 3).

Typical curves of lift coefficient plotted against angle of attack are shown for Mach numbers of 0.89 and 1.25 in figure 7. The curves are smooth and show a linear variation of lift coefficient with angle of attack within the range tested. The data also show a displacement of the lift variation with angle of attack for an increasing and decreasing lift. The hysteresis-like effects presented in figure 7 result from a time difference between the angle of attack and normal acceleration of from 0.002 to 0.004 second or an instrument phase difference of from 3° to 5°. However, an investigation of the instrument responses did not explain a phase lag of this magnitude. Aerodynamic calculations have shown that only part of the apparent hysteresis (less than 25 percent) can be attributed to the lift proportional to pitching velocity and the lift proportional to the angle-of-attack variation with time. Similar hysteresis-like effects were noted in drag and hinge-moment responses and have been observed on two other pulsed-control models reported in references 1 and 4. Other configurations have been free of this effect.

The variation of lift-curve slope C_{L_α} with Mach number is shown in figure 8. The values of C_{L_α} obtained are average slopes between angles of attack of 1° and 6°. A linear lift-curve slope was indicated for this angle-of-attack range within the accuracy of the data. The results show a gradual variation of C_{L_α} with Mach number. The maximum lift-curve slope was 0.057 at a Mach number of 1.05.

The damping of the oscillations is indicated by the exponential damping constant b, as shown in the appendix. The values of b are shown for the flight test conditions in figure 9. The time to damp to one-half amplitude may be determined from the relationship $T_{1/2} = \frac{0.693}{b}$. At supersonic velocities $T_{1/2}$ would be about 0.2 second as compared to 0.35 second at subsonic velocities. The values of the damping-in-pitch derivative $C_{m_q} + C_{m_{\dot{\alpha}}}$ were determined from the values of b and are shown as a function of Mach number in figure 10. A decrease in the damping in pitch from subsonic and supersonic values is indicated at a Mach number of about 1.0. The value of $C_{m_q} + C_{m_{\dot{\alpha}}}$ was -0.22 at a Mach number of 1.25. A comparative value at a Mach number of 1.25 for a

conventional unswept-tapered-wing configuration is -0.29 (reference 4), and for a tailless-delta-wing configuration the value of $C_{m_q} + C_{m_{\dot{\alpha}}}$ is -0.04 at the same Mach number (reference 5).

The static stability is a function of the frequency or period of the short-period oscillation. The periods measured from the short-period oscillations obtained in flight are shown from a Mach number of approximately 0.7 to 1.45 in figure 11. The curve shows the decrease in period, or the increase in static stability with increasing Mach number. A slower decrease in period at supersonic speeds is shown with a slight irregular variation indicated at a Mach number of 0.93. The damped natural frequency of the configuration varied from 1.8 cycles per second at a Mach number of 0.74 to 4.4 cycles per second at a Mach number of 1.45. The static pitching-moment derivative C_{m_α} was obtained from the plot of period against Mach number and is shown in figure 12. A rapid increase in static stability is indicated at a Mach number of 0.93 and a maximum value is reached at a Mach number of 1.05.

The aerodynamic center of the missile was determined from the static stability derivative and lift-curve slope. The variation of aerodynamic-center position with Mach number is shown in figure 13. The value of the aerodynamic-center position is expressed in percent of the wing mean aerodynamic chord. The aerodynamic center was located 24 percent ahead of the leading edge of the mean aerodynamic chord at a Mach number of 0.9. A gradual rearward shift of the aerodynamic center of 12 percent of the mean aerodynamic chord occurs between Mach numbers of 0.9 and 1.25 and is followed by a gradual forward shift with increasing supersonic velocities.

Control effectiveness.- The effectiveness of the canard control surfaces in producing model lift and in producing a pitching moment is illustrated in figures 14 and 15. The lift produced by control deflection $C_{L_{\delta_e}}$ was small throughout the test Mach number range. The accuracy of $C_{L_{\delta_e}}$ is low, since it is a small percent of C_{L_α}. However, a negative value of $C_{L_{\delta_e}}$ indicates that the negative wing lift caused by downwash from the deflected canard surfaces was larger than the positive lift produced by the control surfaces themselves.

Pitching effectiveness, represented by the derivative $C_{m_{\delta_e}}$, was positive through the Mach number range tested in flight. The increase in downwash above a Mach number of 0.9, which was indicated in the reversal of the values of $C_{L_{\delta_e}}$, is evidenced in the increased values of $C_{m_{\delta_e}}$ at supersonic speeds. Since the wings on this configuration

are well behind the center of gravity, the negative wing lift produced a pitching moment which added to the pitching moment produced by lift on the control surfaces. Thus, it can be seen that nearly all of the canard missile lifting response results from the angle of attack produced by control-surface deflection.

The canard control-surface lift and pitching-moment derivatives were obtained from the trim lift and trim angle-of-attack variations obtained in flight (see appendix). The trim lift coefficients and the trim angles of attack are shown as functions of Mach number for a control deflection of 5° in figures 16 and 17. Small out-of-trim values, occurring at $\alpha = 0^\circ$ and $\delta = 0^\circ$ and probably resulting from slight asymmetries in model construction, have been subtracted from the curves. The increase in trim angle of attack and trim lift coefficient shown between Mach numbers of 0.8 and 0.9 is to be expected since control pitching effectiveness and lift-curve slope were increasing and static stability was decreasing in this range.

The steady-state normal accelerations and angles of attack are shown in figures 18 and 19 for a unit control deflection. Calculated values of $\frac{\Delta a_n/g}{\Delta \delta_e}$ are shown at sea level and at 20,000 feet and show the ability of the configuration to produce steady-state lifts. The effect of altitude can be seen in the curves of normal acceleration per unit control deflection. The values of $\frac{\Delta a_n/g}{\Delta \delta_e}$ and $\frac{\Delta \alpha}{\Delta \delta_e}$ vary inversely as the stability of the missile, a more rearward center-of-gravity location producing higher maneuverability $\left(\frac{\Delta \alpha}{\Delta \delta_e} \text{ and } \frac{\Delta a_n/g}{\Delta \delta_e}\right)$.

Hinge moments.- Control-surface hinge moments were measured in flight about a hinge line at the 64 percent root chord. Maximum hinge moments obtained in flight were 18 inch-pounds for $\alpha = 6.3^\circ$ and $\delta_e = 5^\circ$ at a Mach number of 1.4 and, 70 inch-pounds for $\alpha = 9.1^\circ$ and $\delta_e = 5^\circ$ at a Mach number of 0.89.

Hinge-moment coefficients were obtained as a function of angle of attack for the constant control deflection of 5° and are plotted in figure 20 for a Mach number range of 0.85 to 1.45. The results show a nearly linear variation of C_h with α at the lowest and highest Mach numbers tested, but nonlinear slopes are noted between Mach numbers of 0.88 and 1.0. The average slopes were measured and the variation of C_{h_α} with Mach number is shown in figure 21. The larger value of C_{h_α}, 0.007 at $M = 0.8$, as compared with an average value of 0.002 at supersonic

speeds, indicates the subsonic control-surface aerodynamic center was farther forward from the hinge line than was the supersonic aerodynamic center.

The average slope of hinge-moment coefficient with control deflection, as determined from C_{h_α} and the trim hinge-moment coefficients, is plotted against Mach number in figure 21. The center of pressure due to control deflection was ahead of the hinge line at subsonic speeds and shifted rearward at a Mach number of about 0.9. A center of pressure behind the hinge line was indicated at Mach numbers greater than 1.15. An interesting comparison of magnitudes is afforded by data obtained on a trailing-edge flap on a 60° delta wing and reported in reference 5. The $C_{h_{\delta_e}}$ for the all-movable delta control is -0.001 at a Mach number of 1.3. The comparative value of $C_{h_{\delta_e}}$ for the trailing-edge flap was -0.03 at a Mach number of 1.3. A rocket-propelled missile employing a 60° delta variable-incidence wing has been flight-tested, and unpublished hinge-moment data indicate a $C_{h_{\delta_e}}$ of -0.001 at a Mach number of 1.3, comparable to results reported herein. The hinge line was located at 62 percent root chord.

The effect of the body on control-surface hinge moments was indicated by the increment between the curves of C_{h_α} and $C_{h_{\delta_e}}$. The larger positive hinge moments due to angle of attack were probably the results of a more forward center of pressure and a greater lift force caused by upwash from the body.

From the curves of hinge-moment coefficient plotted against angle of attack, C_h at 0° angle of attack and at 0° control deflection were determined, a linear variation of hinge moment with control deflection being assumed. The variation of out-of-trim hinge-moment coefficient with Mach number is presented in figure 22. Except for the Mach number range 1.00 to 1.14, C_{h_0} has a negative value. At a Mach number of 0.8 C_{h_0} represents a hinge moment of 11 inch-pounds or is equivalent to a control deflection of -3°.

Drag.- The primary purpose of this model was to determine the longitudinal stability and control characteristics; however, drag characteristics were also measured and are presented herein.

The variation of drag coefficient with lift coefficient is shown in figure 23 for Mach numbers ranging from approximately 0.8 to 1.45. The induced drag coefficients vary directly with the square of the lift coefficients at subsonic and supersonic velocities. In the transonic region the shape of the curves is altered by the rapid increase of wave

drag with increasing Mach number. Maximum lift-drag ratios and minimum drag coefficients obtained from these curves are shown in figures 24 and 25.

The maximum lift-drag ratio was about 6.5 at a Mach number of 0.75. Lift-drag ratio decreased sharply through the Mach number range of 0.8 to 1.0 and remained constant at a value of about 3.7 at supersonic velocities.

Figure 25 shows the sharp drag rise of the model with the peak minimum drag coefficient of 0.06 occurring at a Mach number of 1.05. $C_{D_{min}}$ decreases gradually with increasing Mach number to a value of 0.047 at a Mach number of 1.45. This high value of $C_{D_{min}}$ results in a lower $(L/D)_{max}$ at Mach numbers greater than 1.0. The minimum drag coefficients are for the condition of zero lift with a 5° control deflection.

CONCLUSIONS

Results of the flight test of a 60° delta wing canard missile configuration indicated a gradual variation and no unusual trends of the longitudinal stability derivatives at transonic and supersonic velocities.

The lift-curve slope and the static stability were linear within the accuracy of the data for the angle-of-attack range ($\pm 6^\circ$) obtained in flight.

Lift-curve slope reached a maximum of 0.057 at $M = 1.05$ and decreased gradually with increasing Mach number. The control surfaces produced a maximum steady-state normal acceleration $\frac{\Delta a_n/g}{\Delta \delta_e}$ of 1.8 at a Mach number of 1.4 at sea level.

The effect of Mach number changes on static and dynamic stability was very small for this configuration. The maximum shift in aerodynamic-center position was 12 percent of the mean aerodynamic chord.

The damping-in-pitch derivative $C_{m_q} + C_{m_{\dot{\alpha}}}$ showed about a 20-percent variation between Mach numbers of 0.9 and 1.25. The time required for the oscillations to damp to one-half amplitude at sea level and supersonic velocities remained constant at about 0.2 second.

Pitching effectiveness of the control surface was maintained throughout the Mach number range with a maximum steady-state α/δ_e of about 0.7

occurring at $M = 0.9$. Lift due to control deflection $C_{L_{\delta_e}}$ was small at all Mach numbers tested. Hence, most of the normal acceleration $\frac{\Delta a_n/g}{\Delta \delta_e}$ was obtained from the angle of attack resulting from deflection of the control surfaces.

Control hinge moments were small throughout the Mach number range tested, the values of C_{h_α} and $C_{h_{\delta_e}}$ never exceeding 0.009. That C_{h_α} and $C_{h_{\delta_e}}$ were restricted to such a small range of values is indicative of the excellent aerodynamic balancing characteristics obtainable with all-movable control surfaces.

Minimum drag coefficient had a peak value of 0.06 at a Mach number of 1.05. Maximum lift-drag ratio was about 3.7 at supersonic velocities.

Langley Aeronautical Laboratory
National Advisory Committee for Aeronautics
Langley Air Force Base, Va.

APPENDIX

METHODS FOR DETERMINING STABILITY, CONTROL, AND HINGE-MOMENT CHARACTERISTICS

The methods for determining stability, control, and hinge-moment characteristics are presented.

The following additional symbols are used:

γ flight-path angle, deg

θ angle of pitch, deg

$C_{L_q} = \frac{\partial C_L}{\partial \frac{q\bar{c}}{2V}}$, per deg

$C_{L_{\dot{\alpha}}} = \frac{\partial C_L}{\partial \frac{\dot{\alpha}\bar{c}}{2V}}$, per deg

C_{L_0} out-of-trim lift coefficient

dC_m/dC_L static margin

$a_1, a_2, a_3, A_1, A_2, A_3, x$ amplitudes used in determining trim line and damping of oscillations

The symbols $\dot{}$ and $\ddot{}$ over a quantity represent the first and second time derivatives, respectively, of the quantity.

The longitudinal stability and control derivatives were obtained by measuring the various angular and translatory responses of the missile to a step input to the control surfaces.

The longitudinal equations of motion for two degrees of freedom are

$$\frac{mV}{57.3qS_w}\dot{\gamma} - C_{L_\alpha}\alpha = C_{L_{\delta_e}}\delta_e \qquad (1)$$

$$\frac{I_y\ddot{\theta}}{57.3qS_w\bar{c}} - C_{m_q}\frac{\bar{c}}{2V}\dot{\theta} - C_{m_{\dot{\alpha}}}\frac{\bar{c}}{2V}\dot{\alpha} - C_{m_\alpha}\alpha = C_{m_{\delta_e}}\delta_e \qquad (2)$$

The following limitations must be observed in the application of the foregoing equations for any particular calculation:

1. The aerodynamic coefficients remain constant.

2. Forward velocity does not change.

3. Disturbances are of small order.

Calculations were made at several Mach numbers to investigate the effect of the terms $C_{L_{\dot{\alpha}}}$ and C_{L_q} on the theoretical responses. In all cases the magnitude of these two terms was negligible compared with the total lift. Since the angular relationship exists,

$$\theta = \alpha + \gamma \qquad (3)$$

the differential equations may be solved for α, θ, γ, or their derivatives when a unit step input is applied to the control surfaces. The solution for any of the variables as obtained from reference 6 has the following form:

$$\alpha(t) = \frac{1}{\omega_{n_d}} e^{-bt}\left(\varphi_b \cos \omega_{n_d} t + \varphi_a \sin \omega_{n_d} t\right) + \alpha_{trim} \qquad (4)$$

This is the equation of a damped sinusoidal variation of α with time, α oscillating about a trim value. The exponential damping constant is b, and the damped natural frequency is ω_{n_d}. The constants φ_b and φ_a are functions of the missile derivatives and depend on the magnitude of the step input.

Lift-curve slope, C_{L_α}.- Lift coefficient is determined by transferring the accelerations measured along the body axes to the stability axes. The angle between the two sets of axes is the missile angle of attack (α). Then

$$C_L = \left(\frac{a_n}{g}\cos\alpha - \frac{a_l}{g}\sin\alpha\right)\frac{W}{qS_w} \qquad (5)$$

The lift-curve slope C_{L_α} is obtained by cross plotting the C_L and α variations with time at a constant control deflection.

Control lifting effectiveness, $C_{L_{\delta_e}}$.- Control lifting effectiveness $C_{L_{\delta_e}}$ is obtained from the variation of trim lift with Mach number. The trim lift coefficient is represented by the following equation:

$$C_{L_{trim}} = C_{L_\alpha}\alpha_{trim} + C_{L_{\delta_e}}\delta_e + C_{L_0} \tag{6}$$

where C_{L_0} is the out-of-trim lift coefficient. Since the controls are pulsed to give positive and negative trim conditions, out of trim can be determined if the assumption is made that C_{L_α} and $C_{L_{\delta_e}}$ are linear within the angle-of-attack range and control deflections obtained

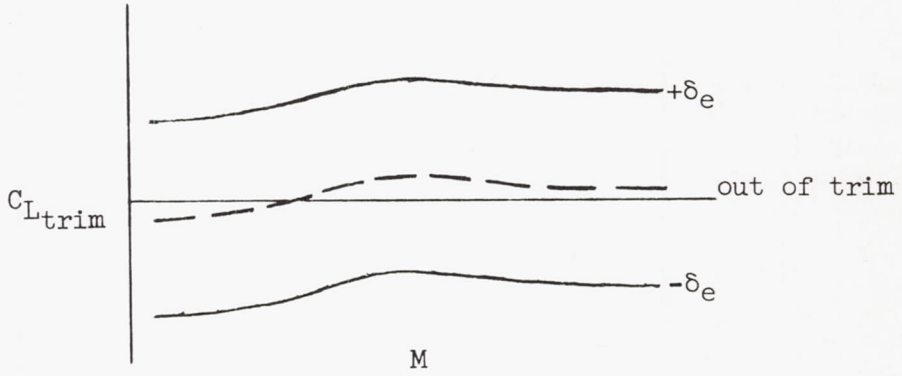

The value of $C_{L_{\delta_e}}$ is then determined from the differences in $C_{L_{trim}}$ for positive and negative control deflections by the following equation:

$$C_{L_{\delta_e}} = \frac{\Delta C_{L_{trim}} - C_{L_\alpha}\left(\Delta\alpha_{trim}\right)}{\Delta\delta_e} \tag{7}$$

It can be seen that the actual slope of $C_{L_{\delta_e}}$ cannot be determined by this technique but the value obtained represents an average slope between the positive and negative control deflections.

Static and dynamic stability.- A typical response of α to a step control input is shown in figure 26.

Before the exponential damping curves can be obtained, a steady-state or trim value of a_n or α must be obtained. This trim value may be determined by any of several methods, two of which are presented here. If at least three or four oscillations are present, an exponential damping curve can be faired through the peak amplitudes and a mean value determined which represents the trim value. The trim value and damping may also be determined over a time interval in which only three peaks are available if it is assumed that the trim value remains constant over this interval.

The exponential damping constant b is determined by measuring amplitude differences from the trim value. Then

$$b = \frac{\ln\left(\frac{A_1}{A_2}\right)}{t_1 - t_2} = \frac{\ln\left(\frac{A_1}{A_3}\right)}{P} \tag{8}$$

By assuming any trim amplitude

$$\frac{a_1 - x}{a_2 + x} = \frac{a_2 + x}{a_3 - x}$$

$$x = \frac{a_1 a_3 - a_2^2}{a_1 + 2a_2 + a_3} \tag{9}$$

where x is the increment between the true and the assumed trim value. The constant ω_{n_d} in equation (4) is simply

$$\omega_{n_d} = \frac{2\pi}{P} \tag{10}$$

The constants ω_{n_d} and b represent the period and damping of the motion and are related to the aerodynamic derivatives and the mass and inertia characteristics of the model. The damping-in-pitch derivative $C_{m_q} + C_{m_{\dot{\alpha}}}$ is related to b in the following manner:

$$C_{m_q} + C_{m_{\dot{\alpha}}} = \left[-\frac{2I_Y}{57.3qS_w\bar{c}} b + \frac{I_Y C_{L_\alpha}}{mV\bar{c}} \right] \frac{2V}{\bar{c}} \tag{11}$$

The static stability derivative is determined by the following relationship:

$$C_{m_\alpha} = - \frac{I_Y}{57.3qS_w\bar{c}}\left(\omega_{h_d}^2 + b^2\right) - \frac{C_{L_\alpha} C_{m_q} \frac{\bar{c}}{2V} 57.3qS_w\bar{c}}{mV\bar{c}} \tag{12}$$

The second term of equation (12) is usually about 1 percent of the value of the first term and, consequently, can be neglected. The static margin and aerodynamic center are then determined by the relationship

$$\frac{dC_m}{dC_L} = \frac{C_{m_\alpha}}{C_{L_\alpha}} \tag{13}$$

Pitching effectiveness.- Pitching effectiveness $C_{m_{\delta_e}}$ is determined from the trim angle-of-attack variation with Mach number

$$C_{m_{\delta_e}} = - \frac{C_{m_\alpha}\left(\Delta\alpha_{trim}\right)}{\Delta\delta_e} \tag{14}$$

Variation of hinge-moment coefficient with angle of attack.- C_{h_α} is obtained by plotting hinge-moment coefficient at a constant control deflection against angle of attack.

Variation of hinge-moment coefficient with control-surface deflection.- $C_{h_{\delta_e}}$ is obtained in a manner similar to $C_{L_{\delta_e}}$, $C_{h_{\delta_e}}$ being an average value between the control deflections tested. If time histories of trim hinge-moment coefficients and trim angles of attack at both positive and negative control deflections are plotted, then an average $C_{h_{\delta_e}}$ is determined from

$$C_{h_{\delta_e}} = \frac{\Delta C_{h_{trim}} - C_{h_\alpha}\left(\Delta\alpha_{trim}\right)}{\Delta\delta_e} \tag{15}$$

REFERENCES

1. Martz, C. William, and Church, James D.: Flight Investigation at Subsonic, Transonic, and Supersonic Velocities of the Hinge-Moment Characteristics, Lateral-Control Effectiveness, and Wing Damping in Roll of a 60° Sweptback Delta Wing with Half-Delta Tip Ailerons. NACA RM L9L14, 1950.

2. Gardiner, Robert A., and Zarovsky, Jacob: Rocket-Powered Flight Test of a Roll-Stabilized Supersonic Missile Configuration. NACA RM L9K01a, 1950.

3. Mitchell, Jesse L., and Peck, Robert F.: An NACA Vane-Type Angle-of-Attack Indicator for Use at Subsonic and Supersonic Speeds. NACA RM L9F28a, 1949.

4. Gillis, Clarence L., Peck, Robert F., and Vitale, A. James: Preliminary Results from a Free-Flight Investigation at Transonic and Supersonic Speeds of the Longitudinal Stability and Control Characteristics of an Airplane Configuration with a Thin Straight Wing of Aspect Ratio 3. NACA RM L9K25a, 1950.

5. Mitcham, Grady L., Stevens, Joseph E., and Norris, Harry P.: Aerodynamic Characteristics and Flying Qualities of a Tailless Triangular-Wing Airplane Configuration As Obtained from Flights of Rocket-Propelled Models at Transonic and Low Supersonic Speeds. NACA RM L9L07, 1950.

6. Churchill, Ruel V.: Modern Operational Mathematics in Engineering. McGraw-Hill Book Co., Inc., 1944.

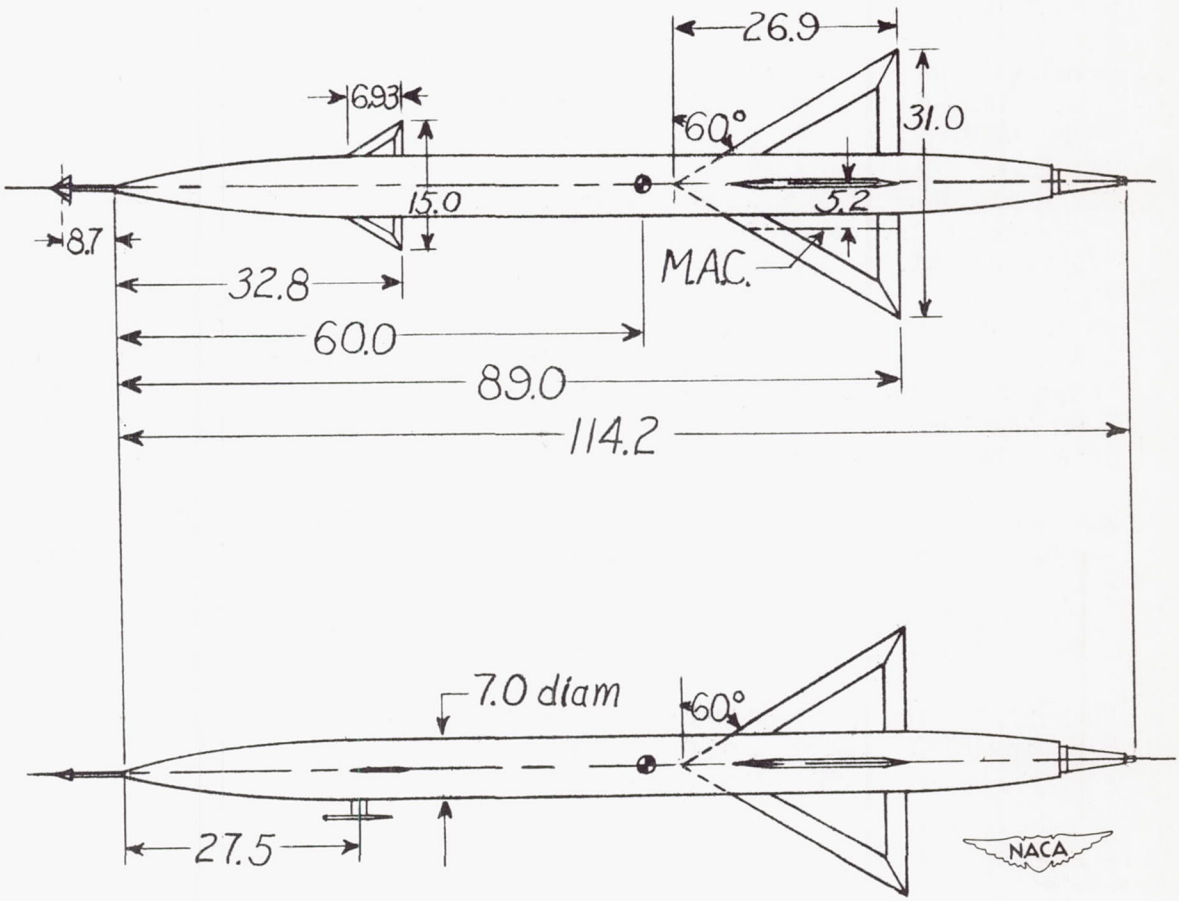

Figure 1.- Model arrangement. (All dimensions are in inches.)

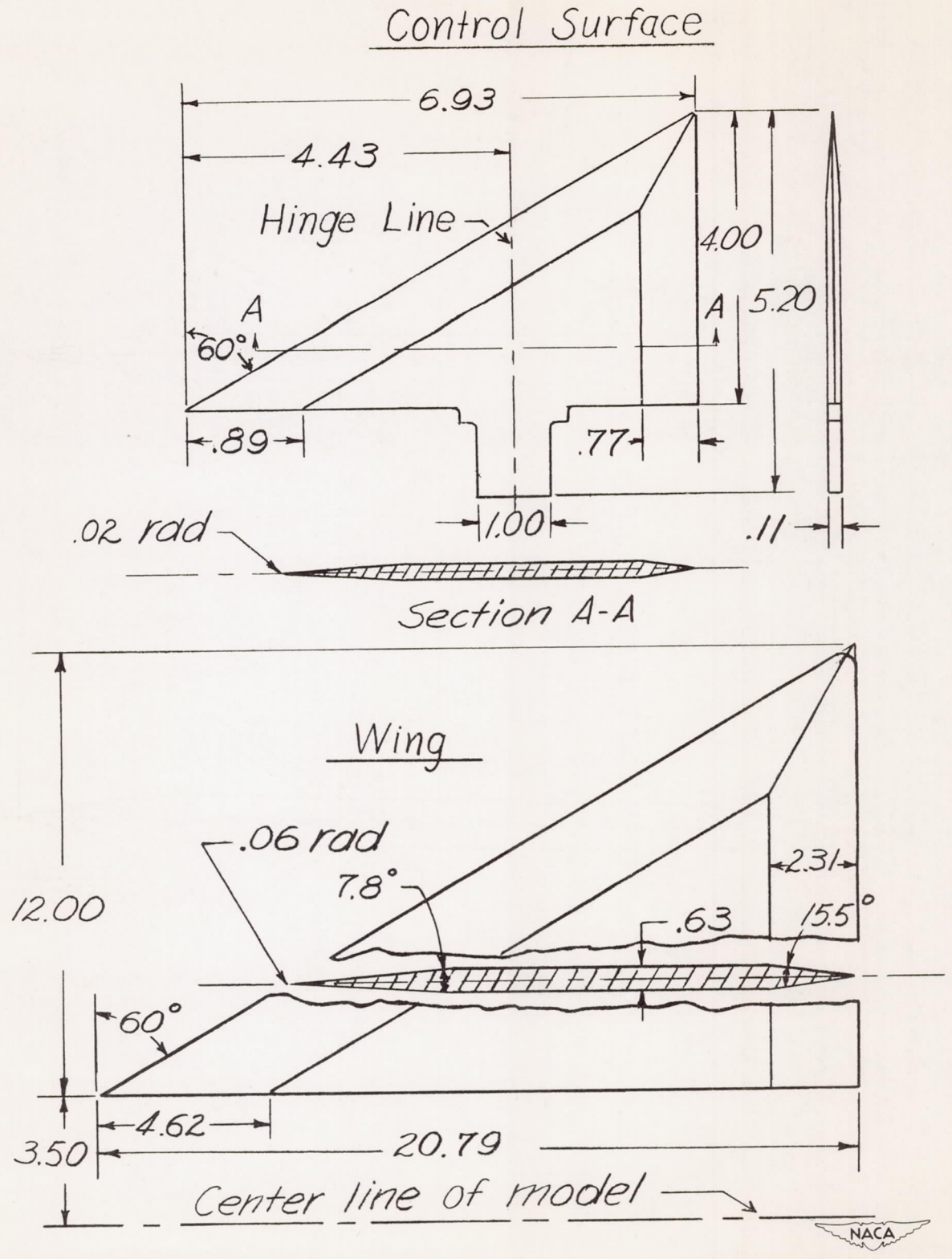

Figure 2.- Wing and control-surface detail. (All dimensions are in inches.)

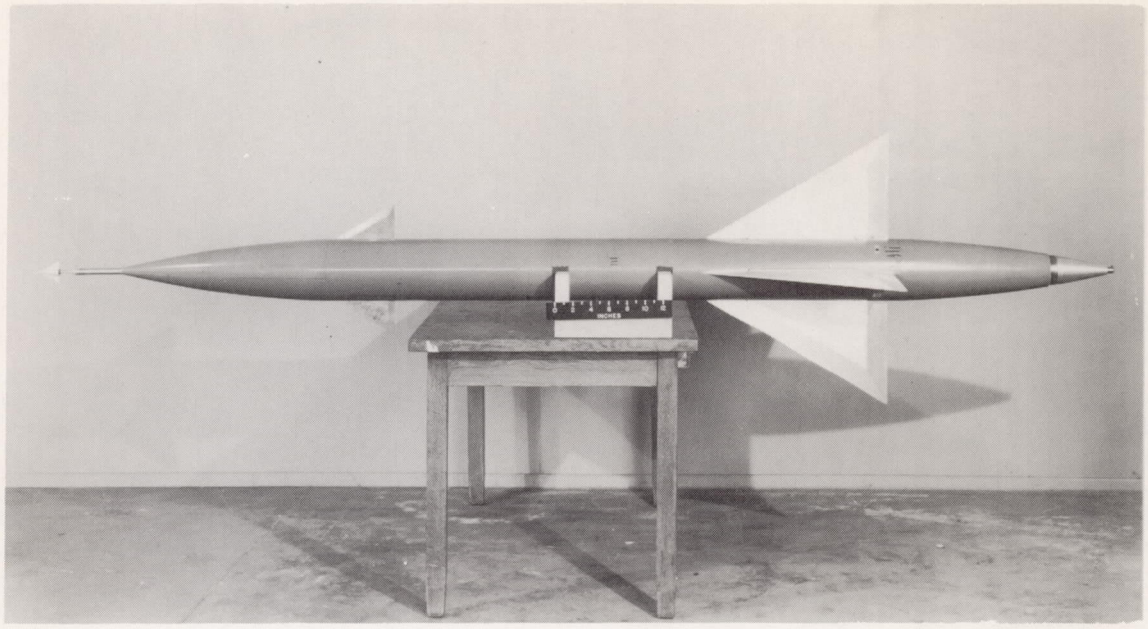

NACA
L-62304

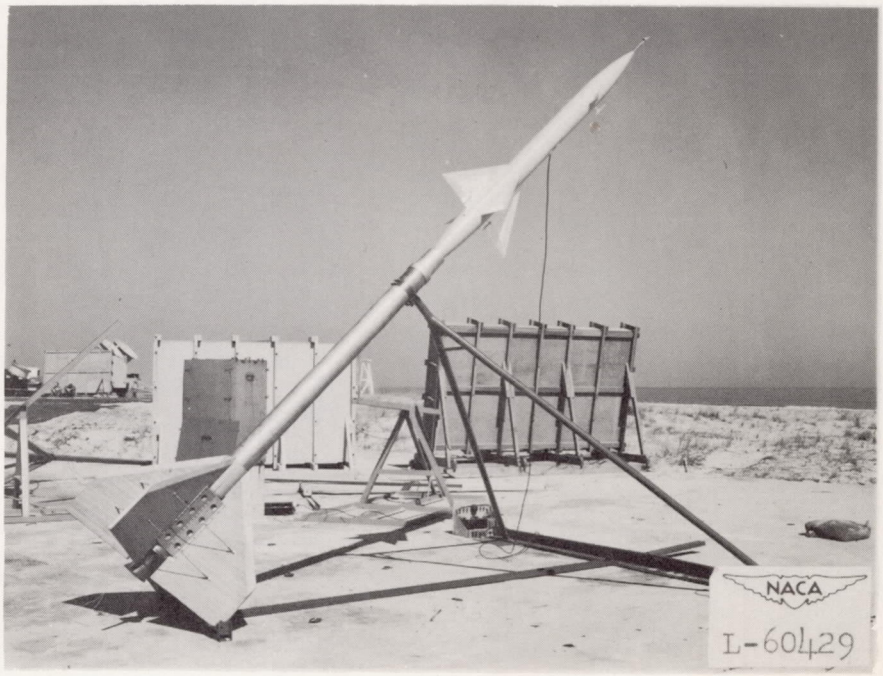

Figure 3.- Model alone and model-booster combination.

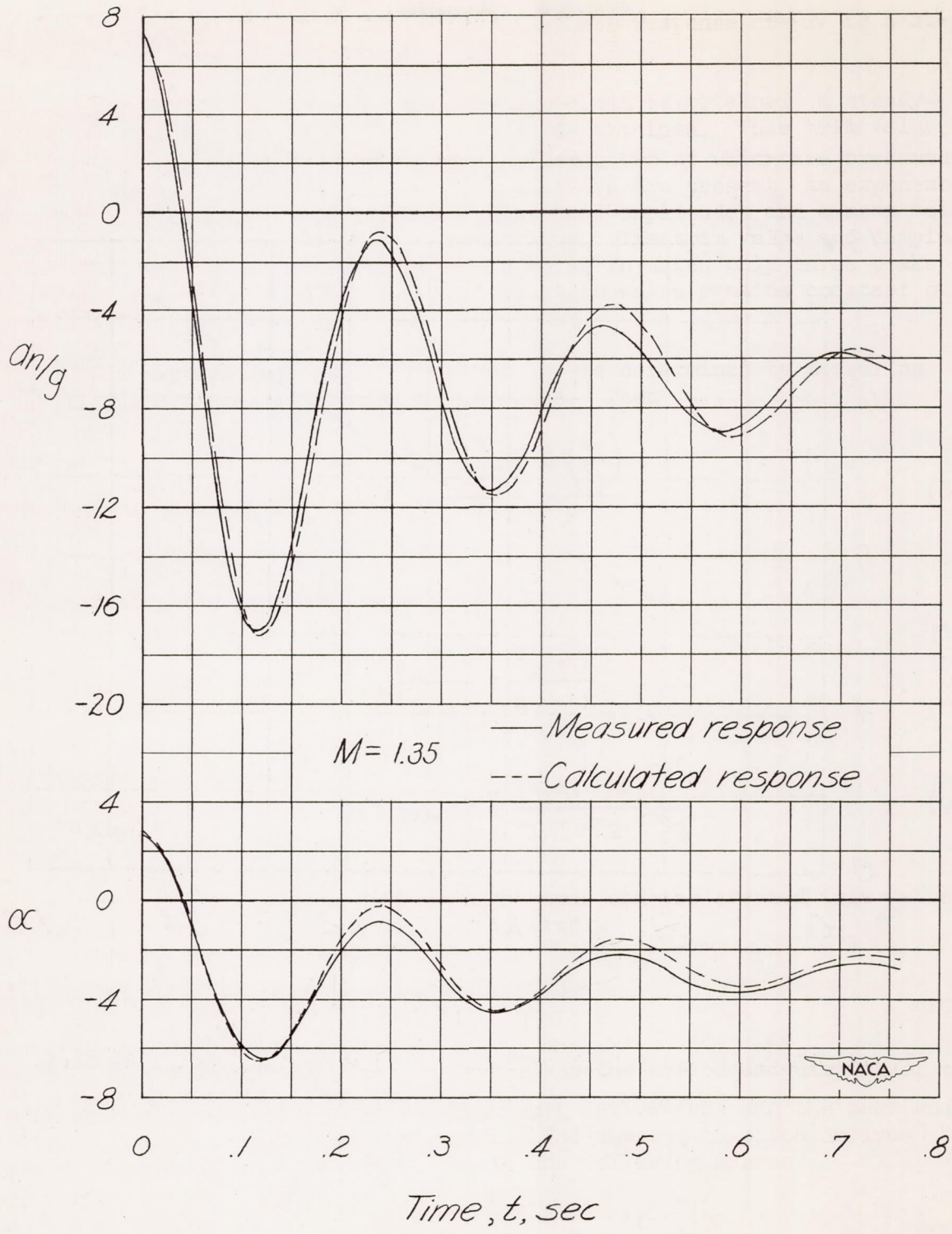

Figure 4.- Comparison of measured and calculated response curves.

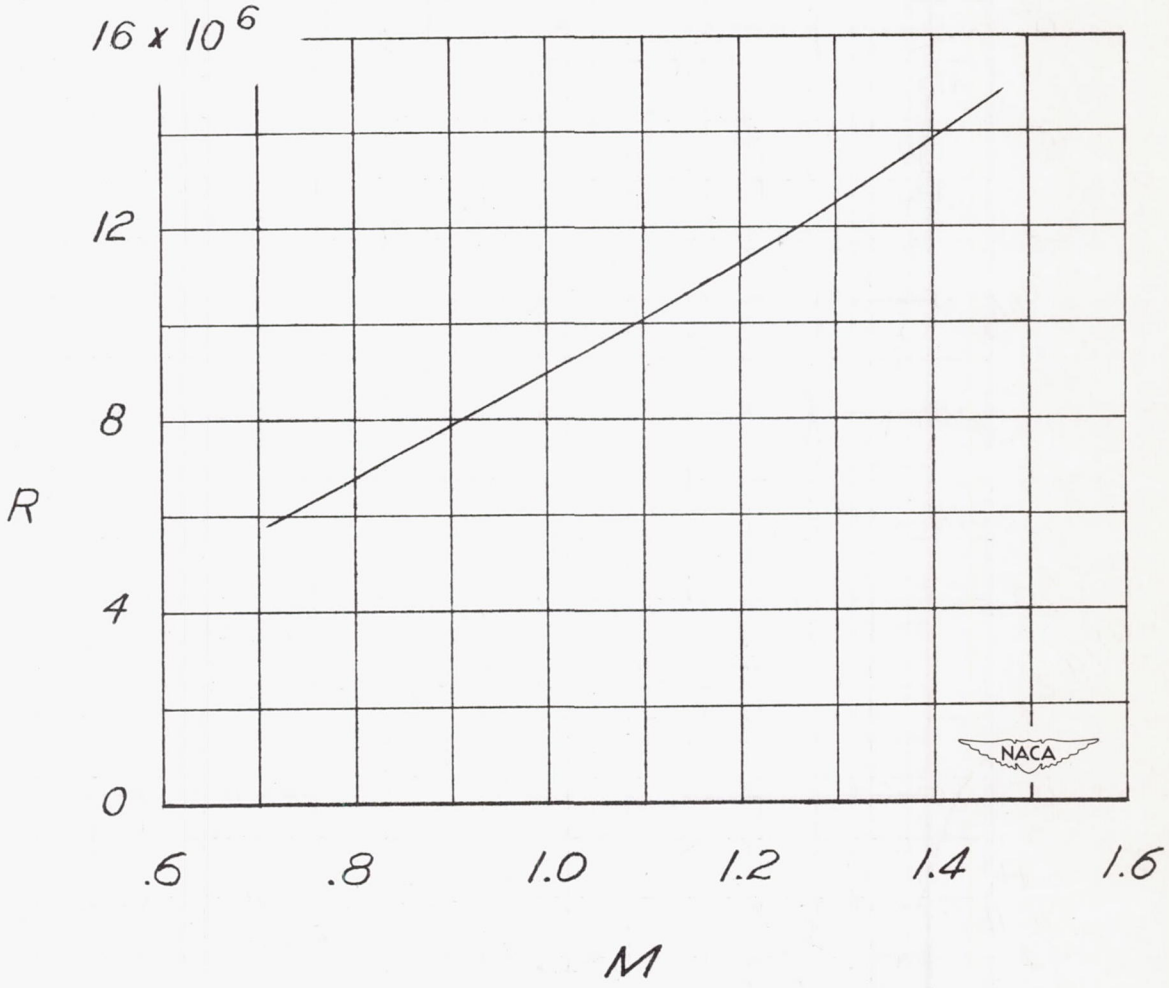

Figure 5.- Scale of flight test, based on wing M.A.C. of 1.49 feet.

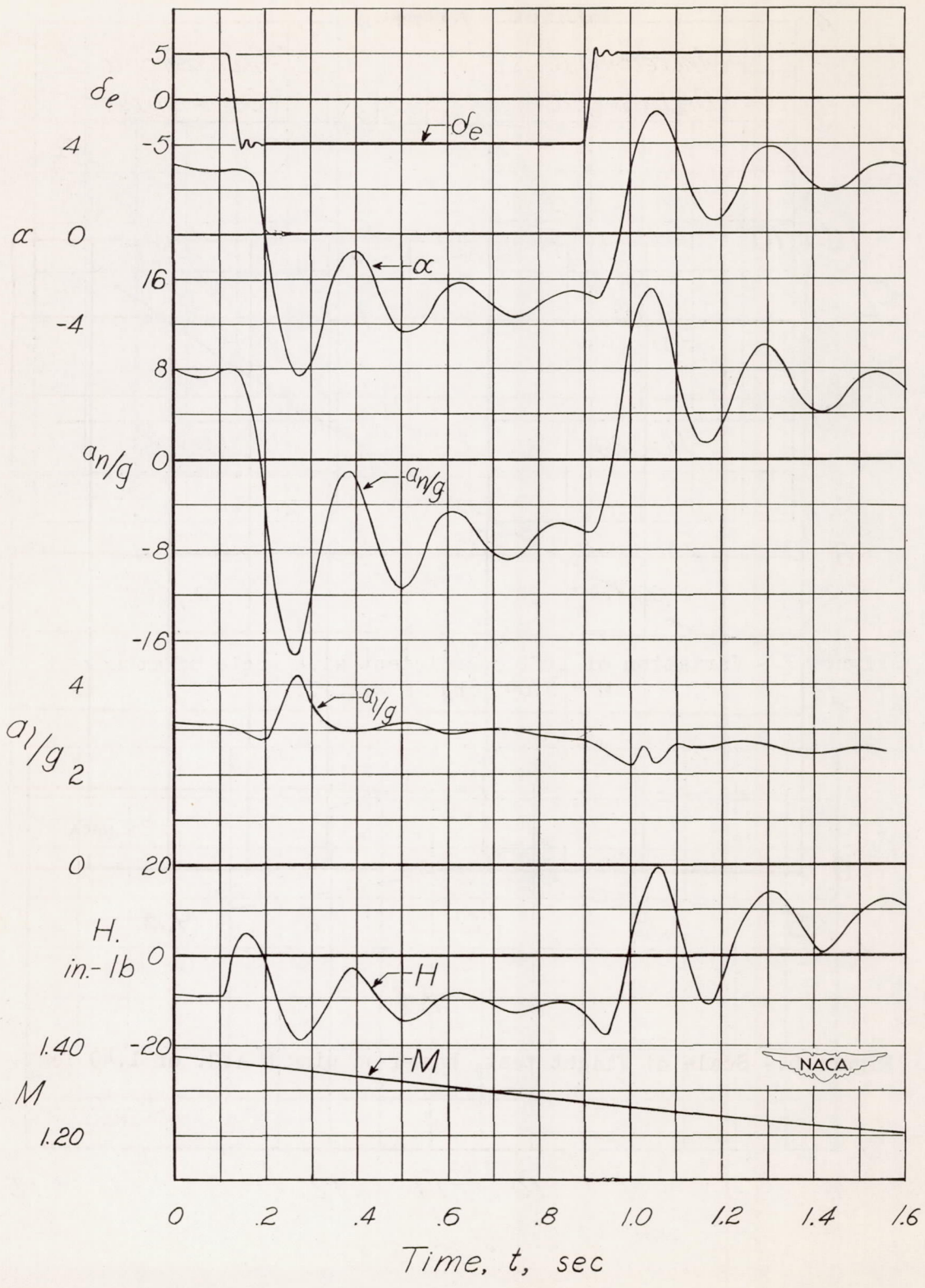

Figure 6.- Sample time history of model flight.

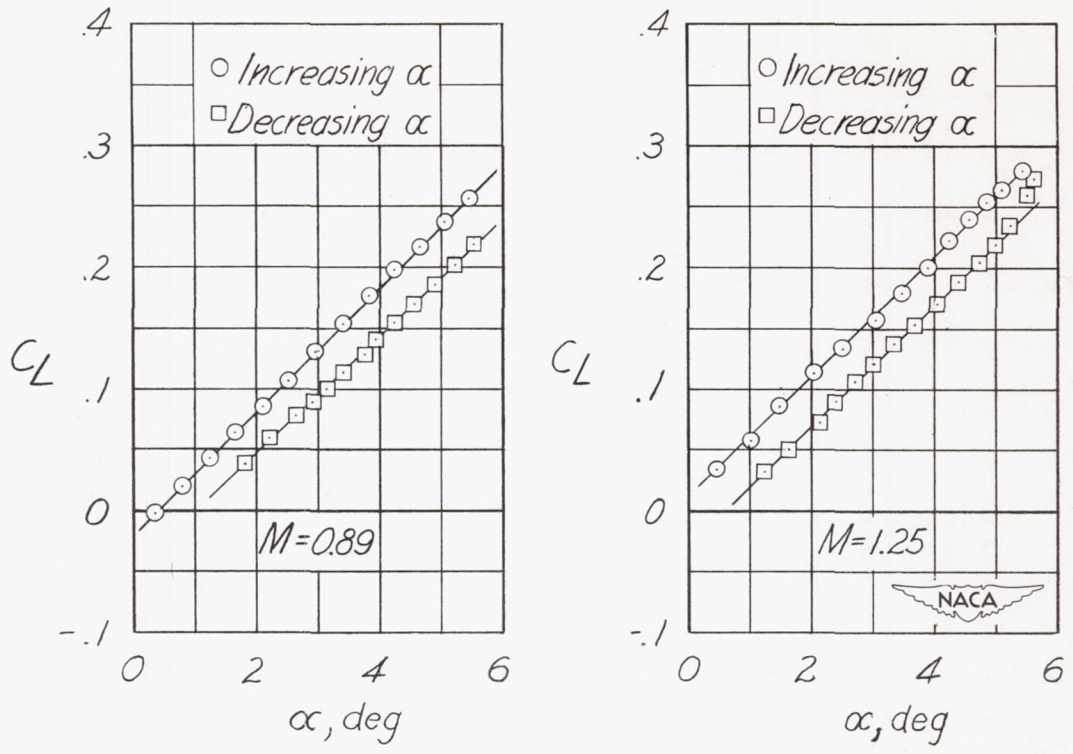

Figure 7.- Variation of lift coefficient with angle of attack at M = 0.89 and M = 1.25.

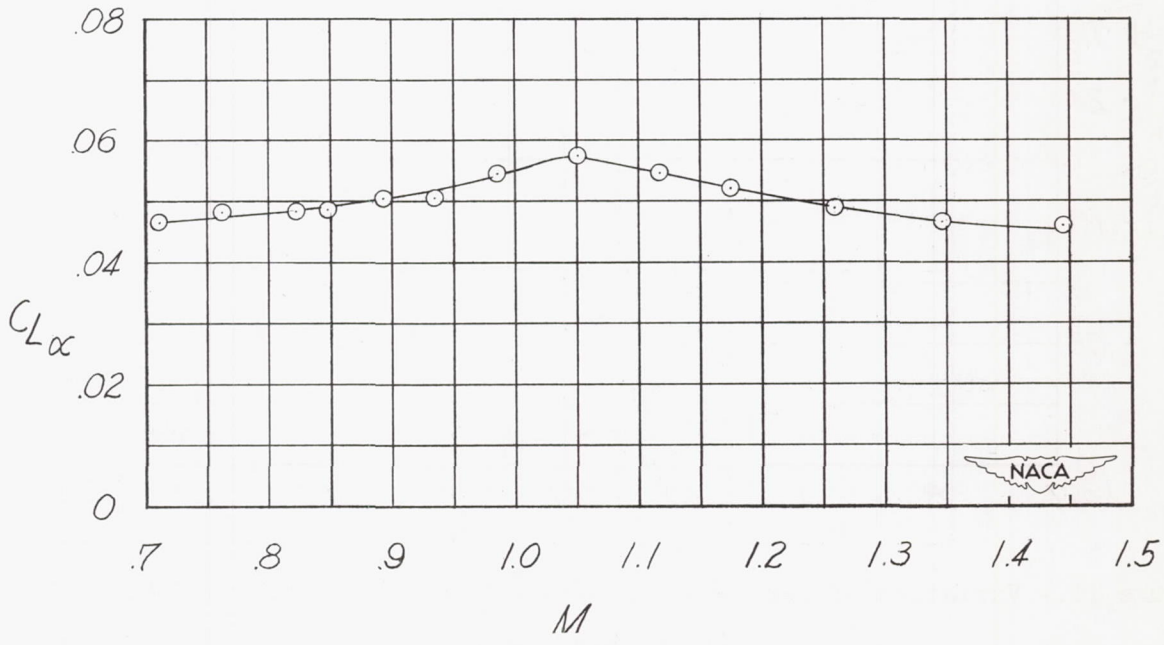

Figure 8.- Variation of lift-curve slope with Mach number.

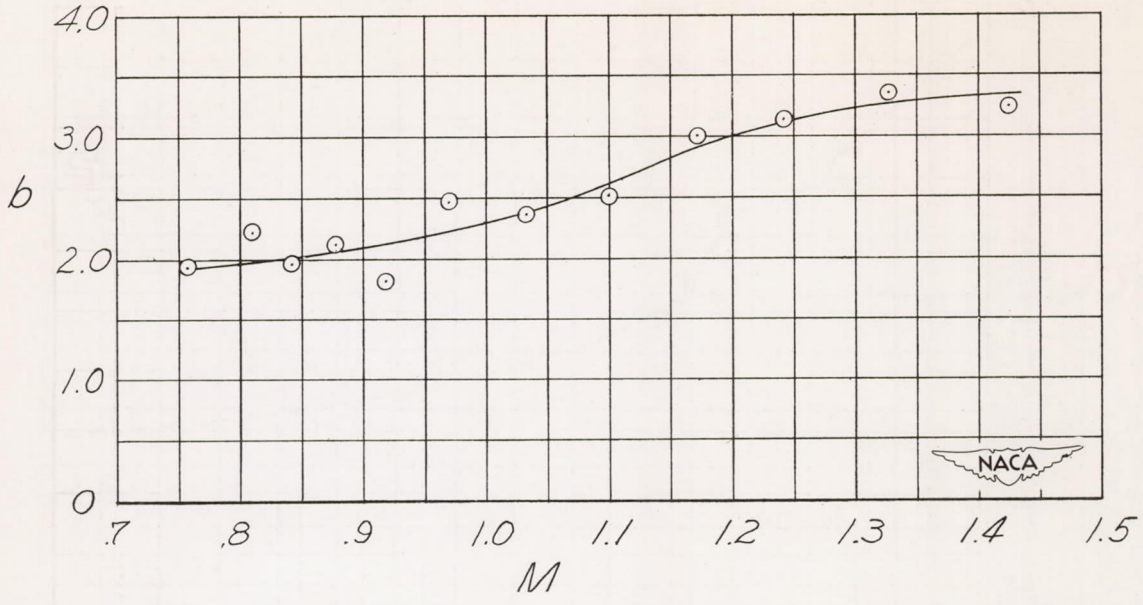

Figure 9.- Variation of exponential damping constant b with Mach number.

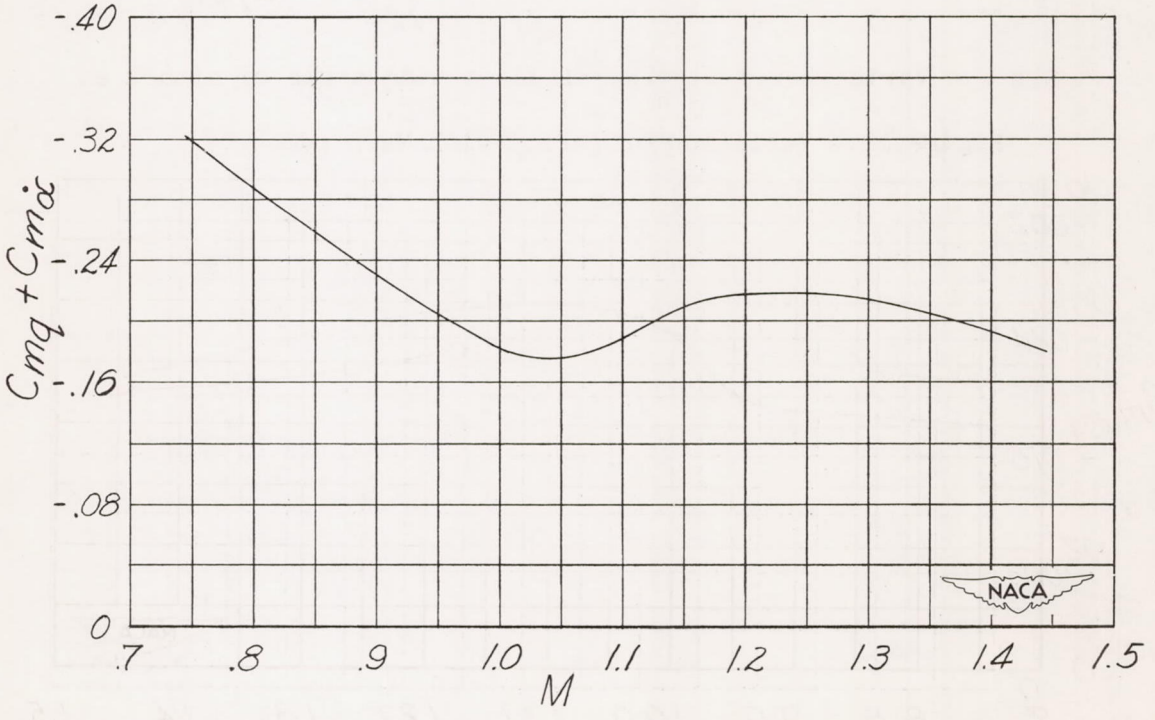

Figure 10.- Variation of aerodynamic damping-in-pitch derivative $C_{m_q} + C_{m_{\dot{\alpha}}}$ with Mach number.

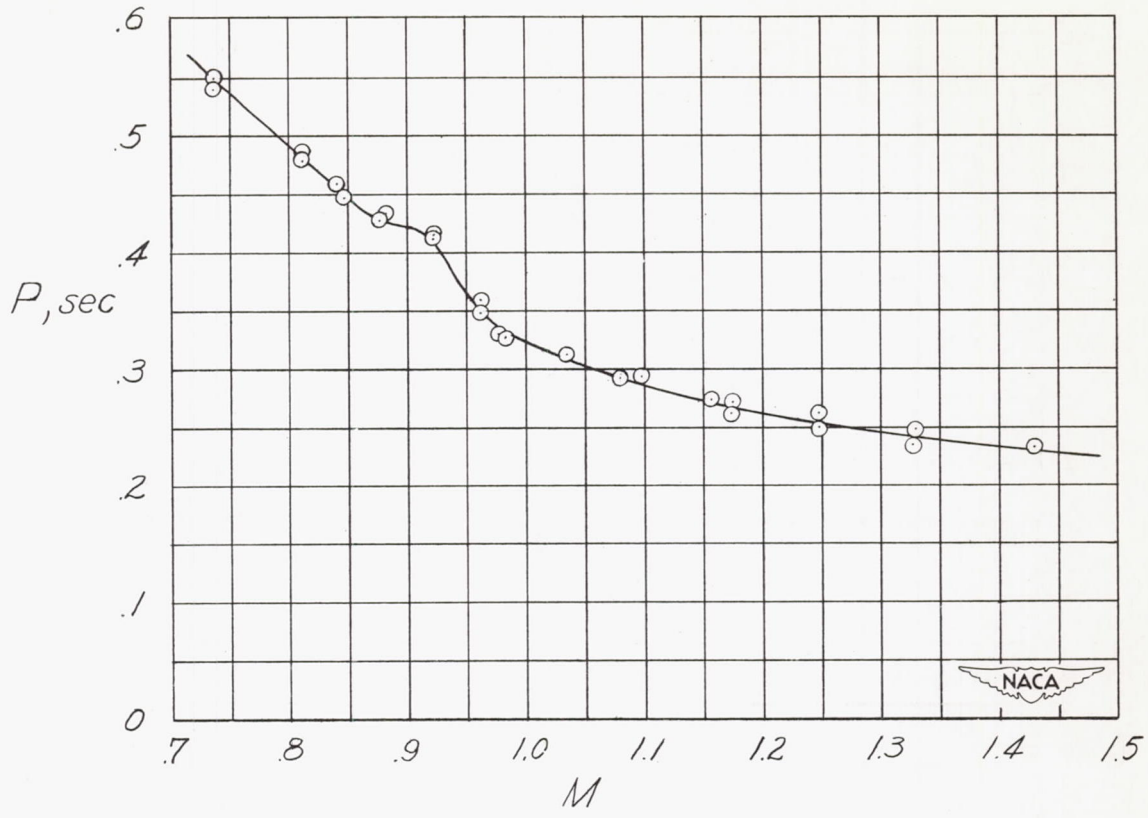

Figure 11.- Variation of period with Mach number.

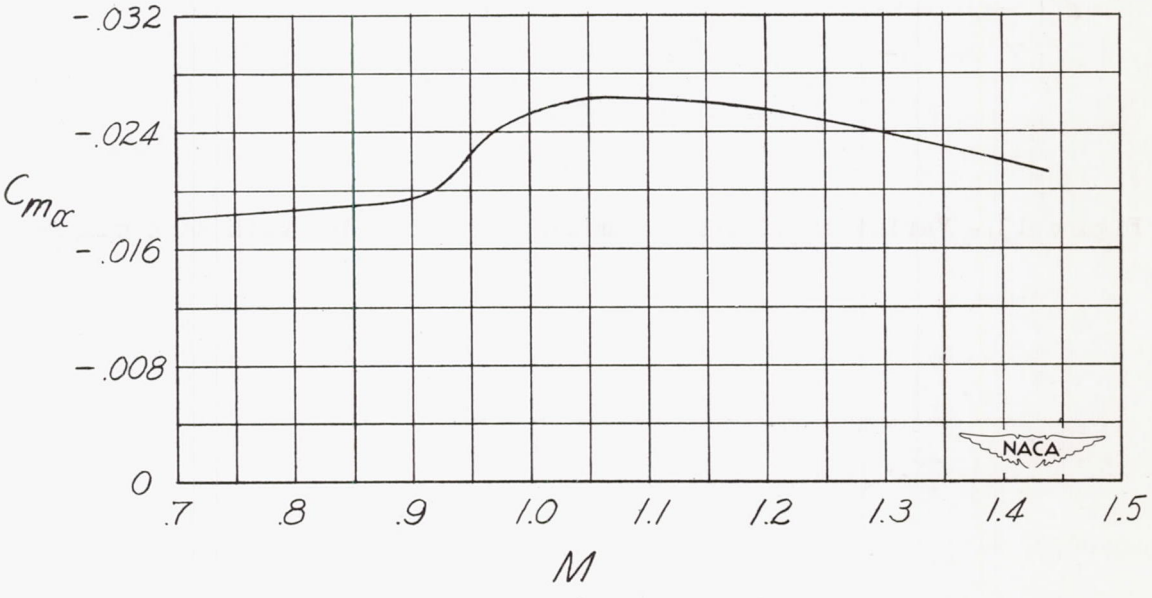

Figure 12.- Variation of static pitching-moment derivative C_{m_α} with Mach number.

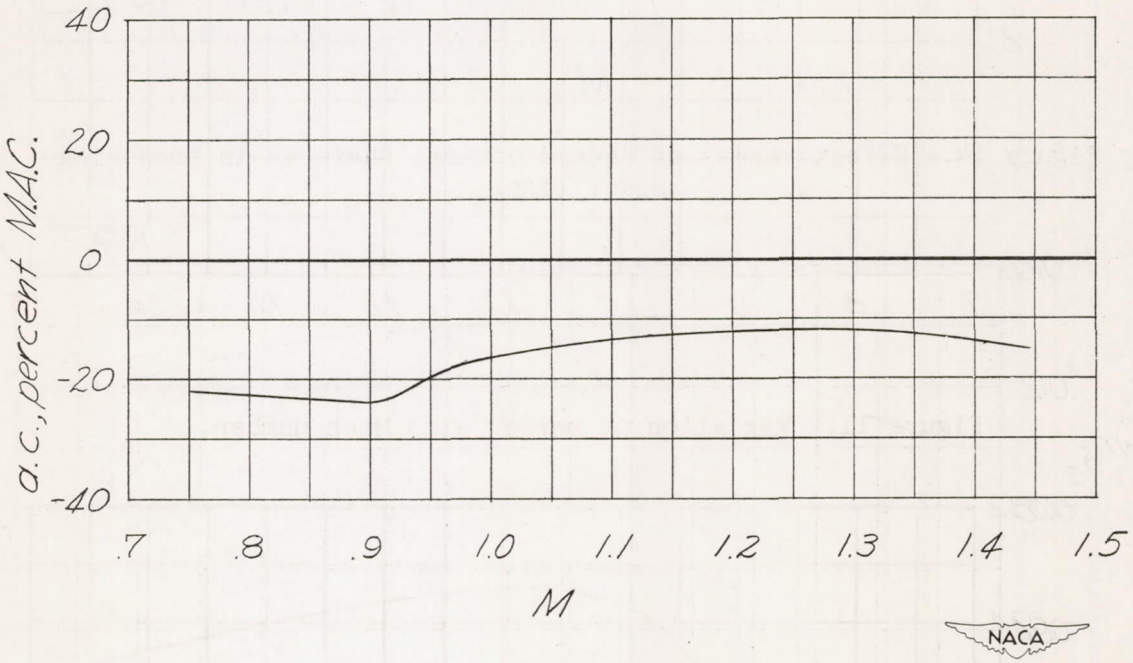

Figure 13.- Variation of aerodynamic-center position with Mach number.

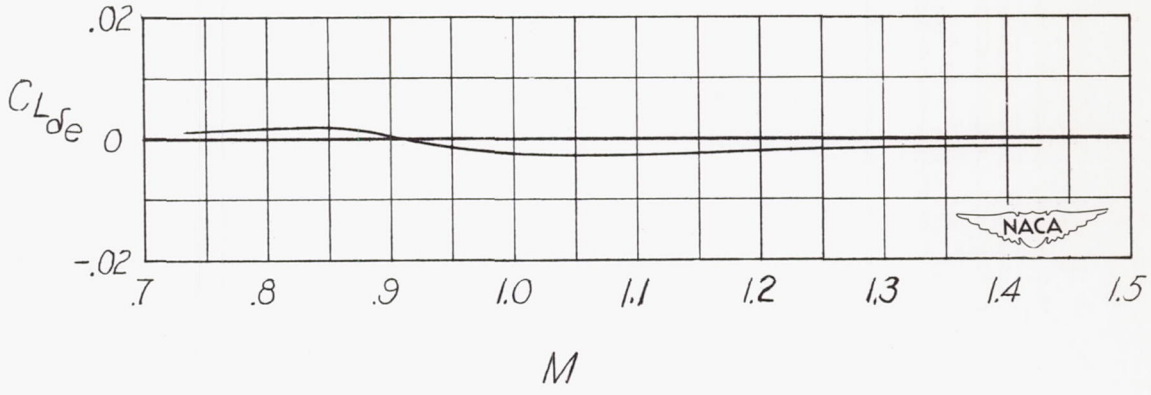

Figure 14.- Effectiveness of canard control surfaces in producing model lift.

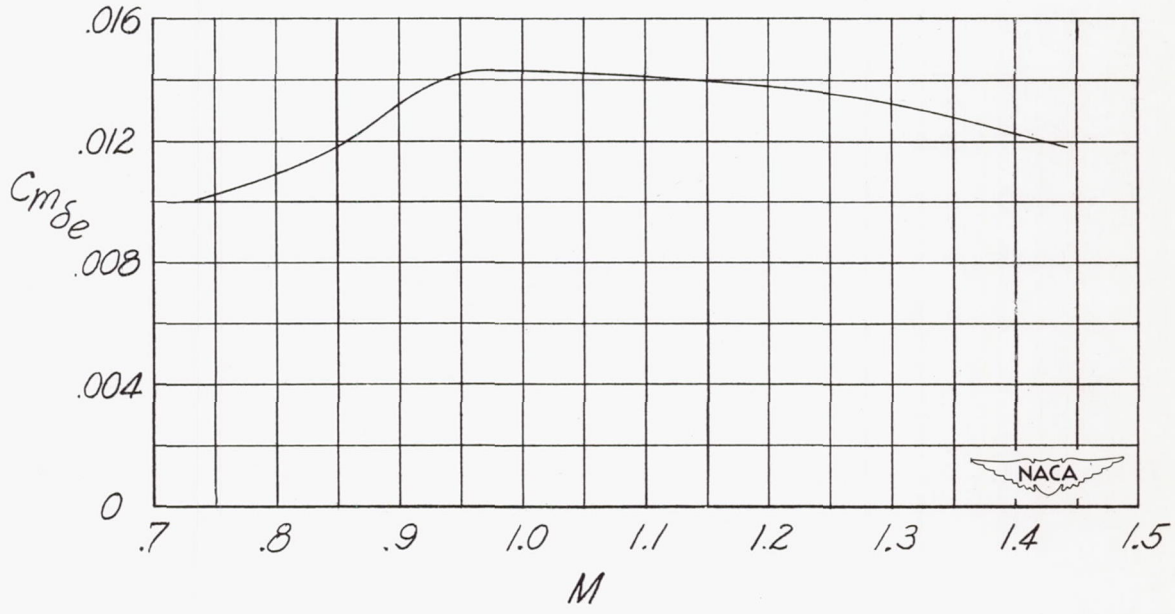

Figure 15.- Pitching effectiveness of canard control surfaces.

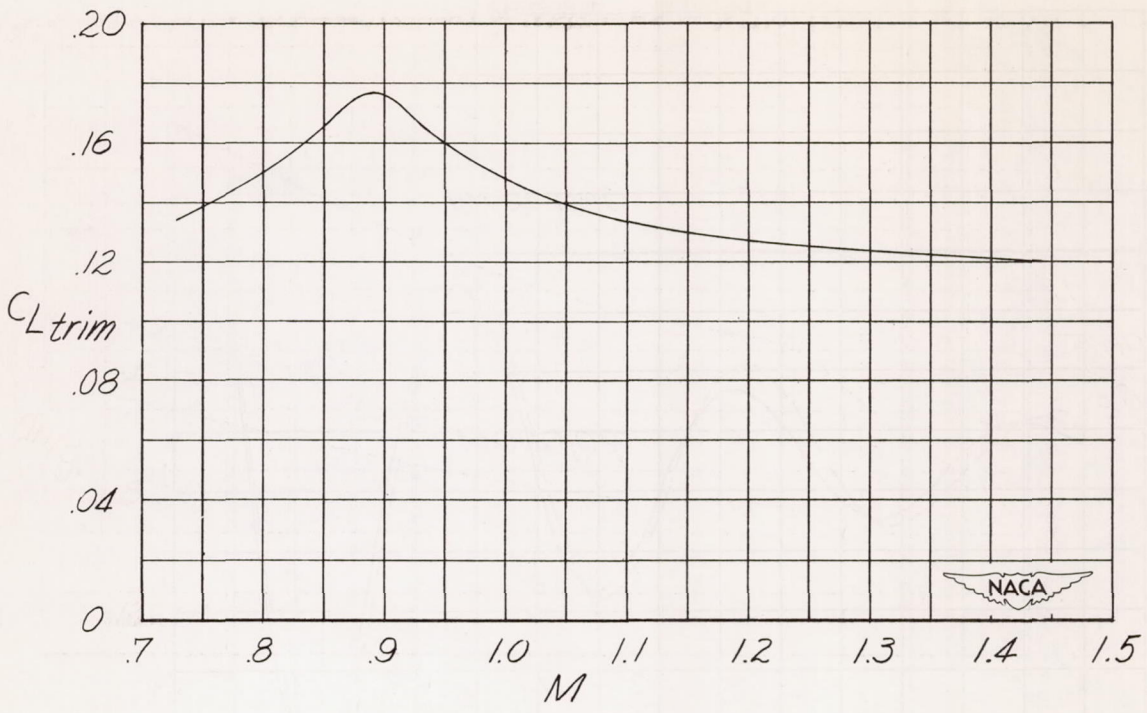

Figure 16.- Variation of trim lift coefficient with Mach number $\delta_e = 5^\circ$.

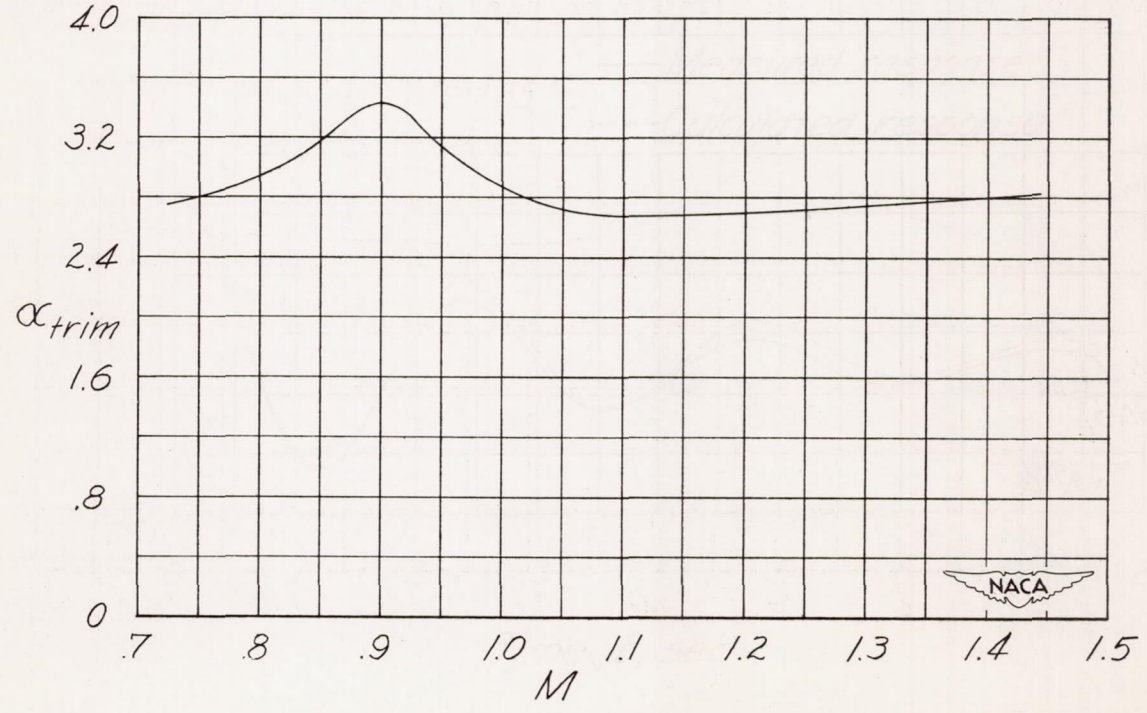

Figure 17.- Variation of trim angle of attack with Mach number $\delta_e = 5^\circ$.

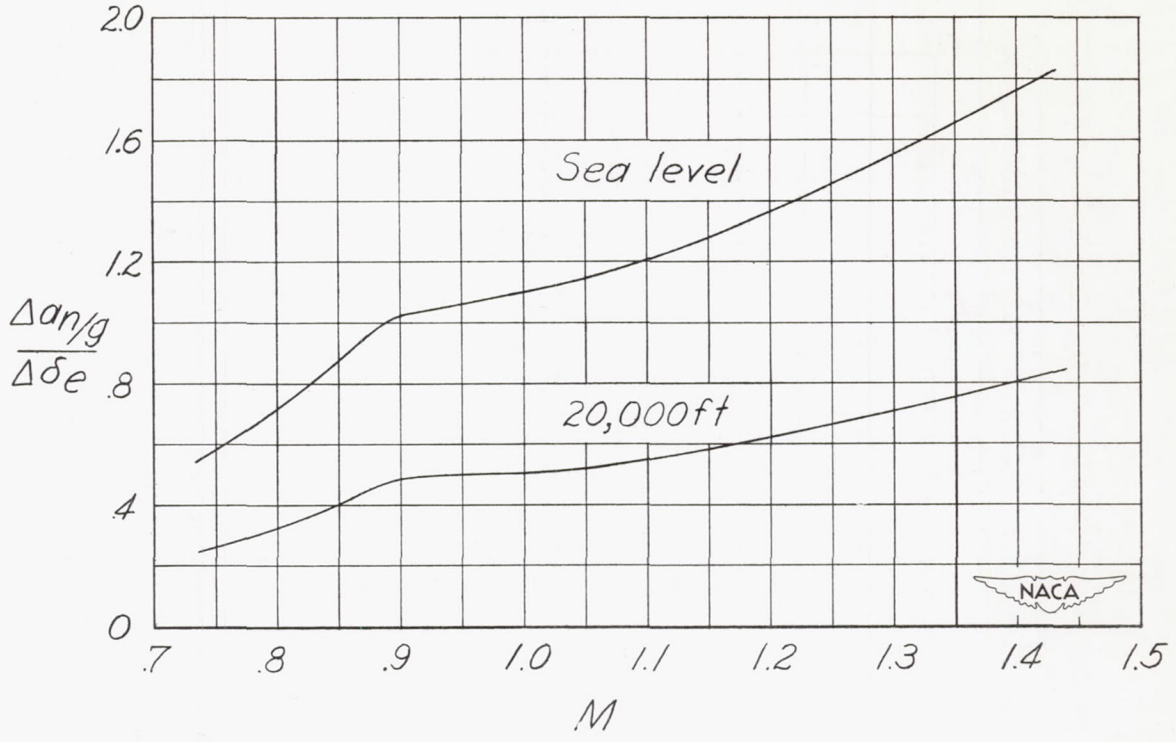

Figure 18.- Trim normal acceleration produced by a unit control deflection.

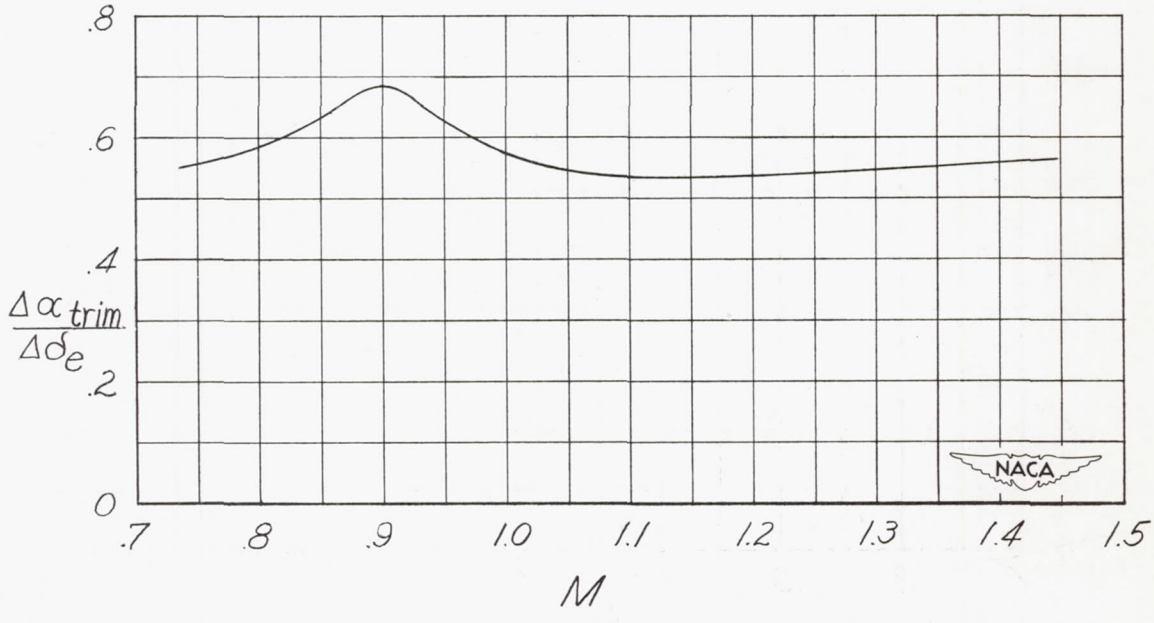

Figure 19.- Trim angle of attack produced by a unit control deflection.

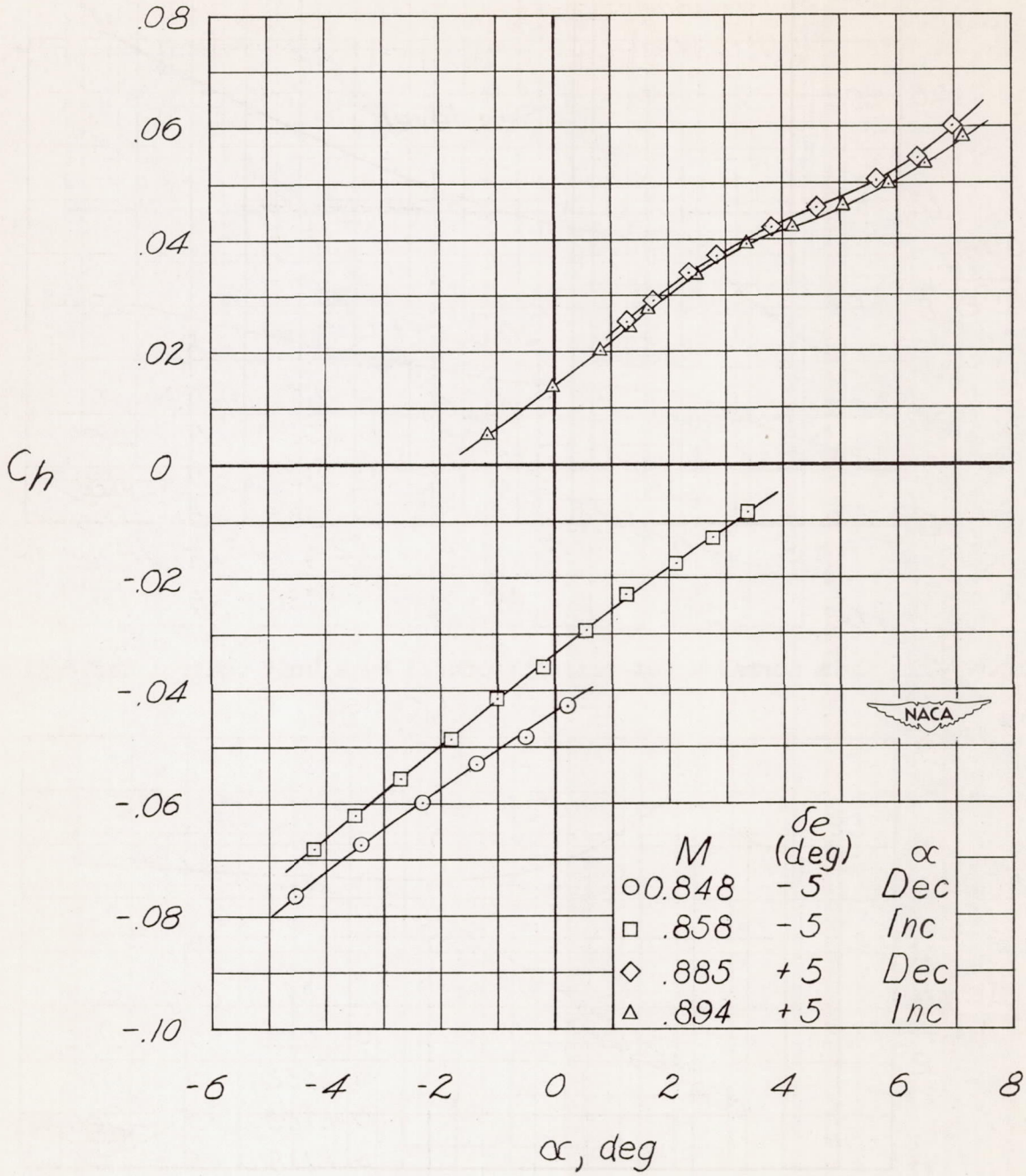

Figure 20.- Variation of control-surface hinge-moment coefficient with angle of attack.

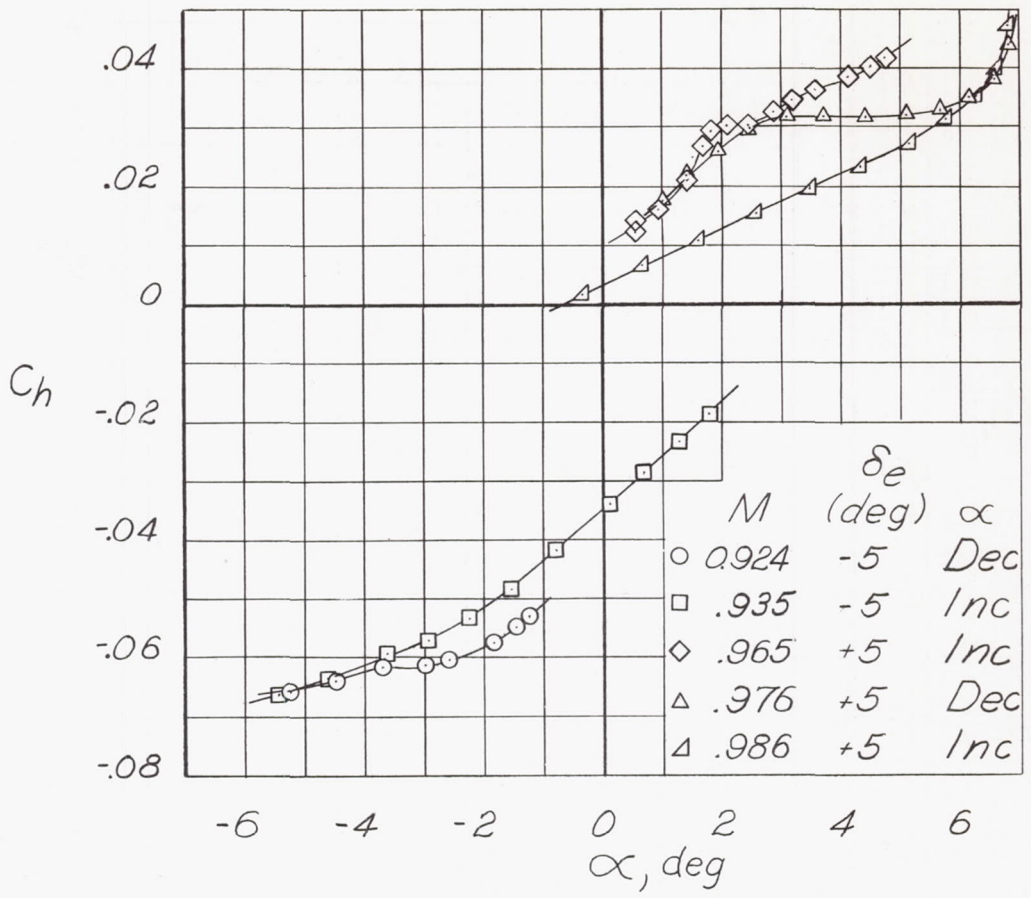

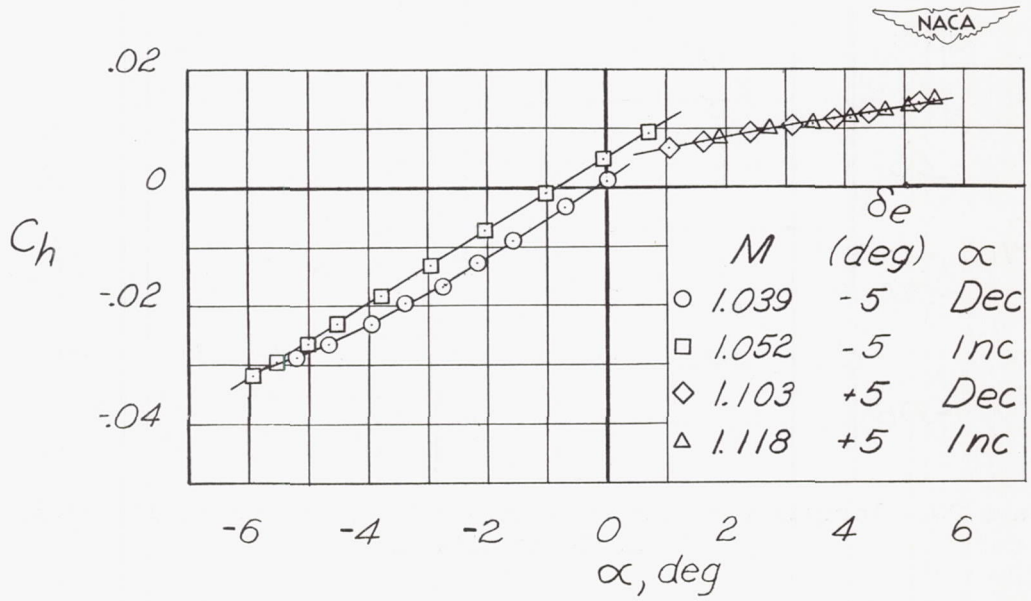

Figure 20.- Continued.

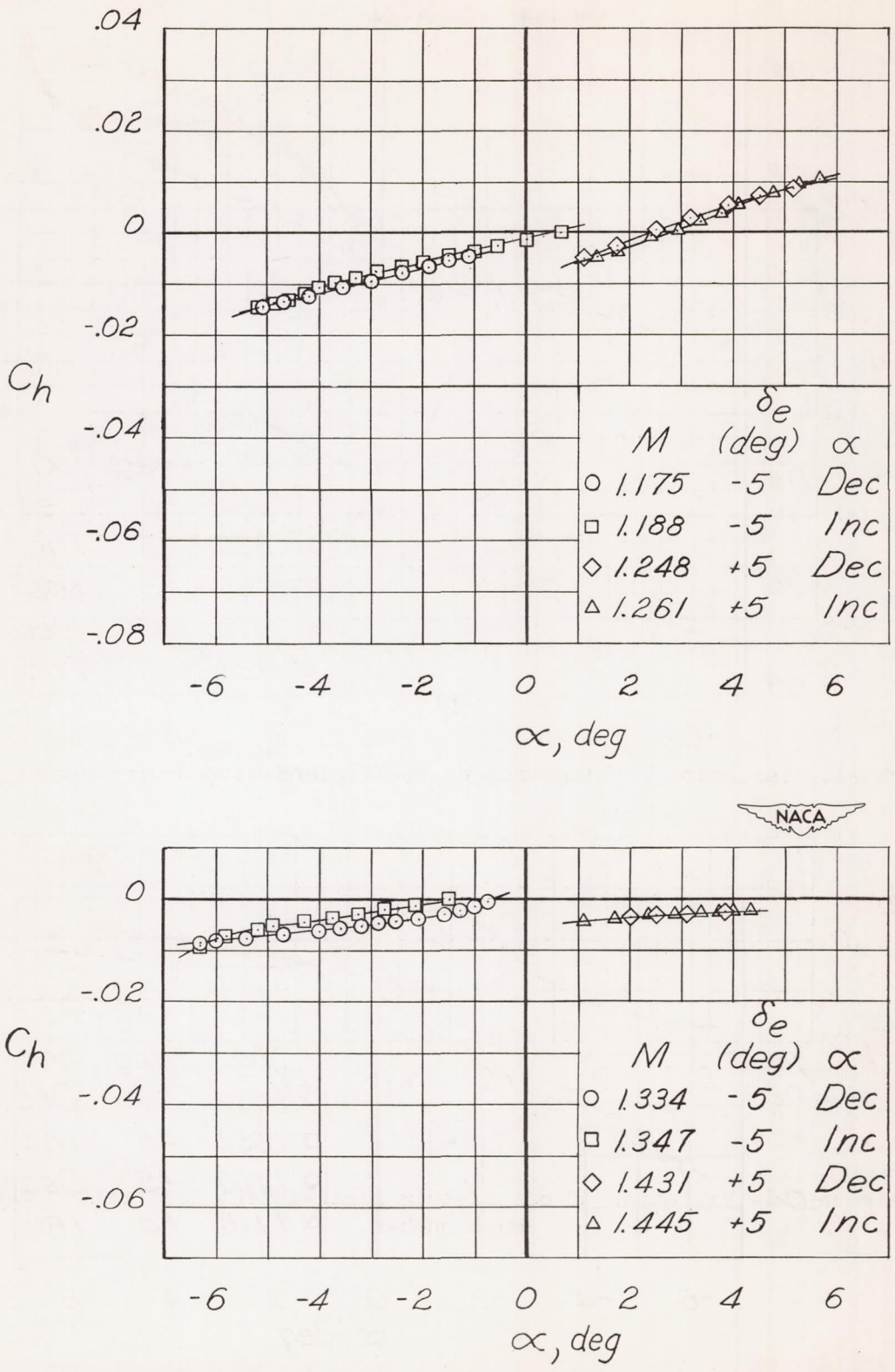

Figure 20.- Concluded.

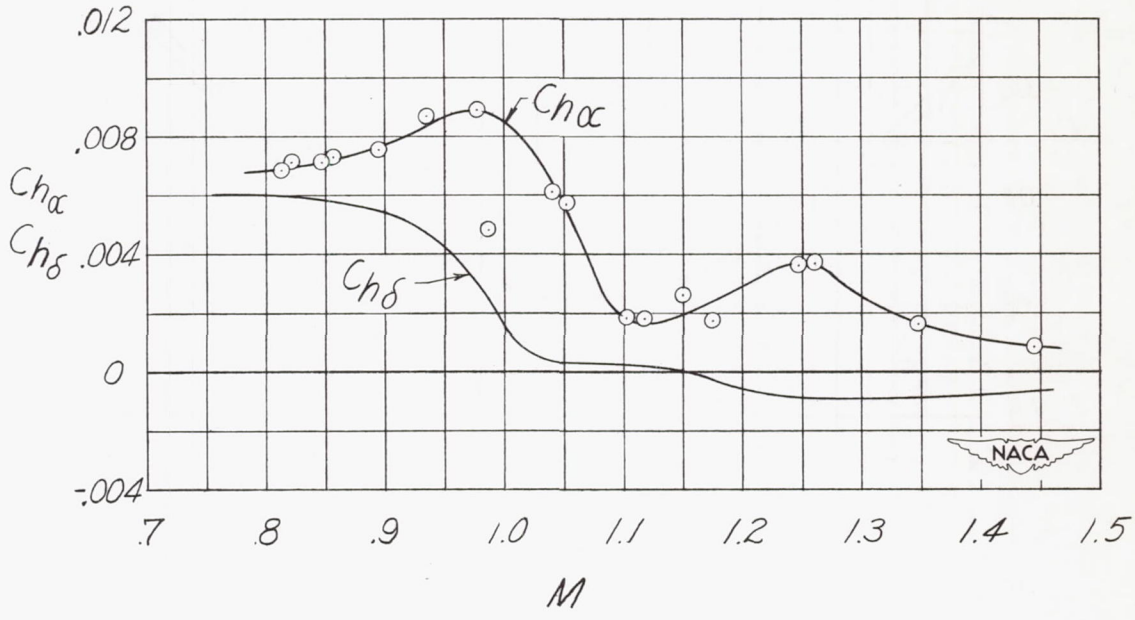

Figure 21.- Variation of hinge-moment-coefficient-slopes with Mach number.

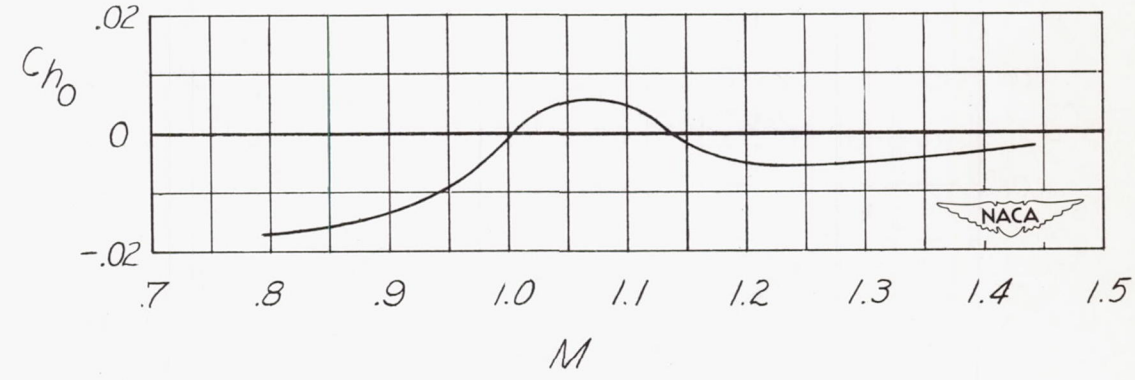

Figure 22.- Variation of out-of-trim hinge-moment coefficient with Mach number.

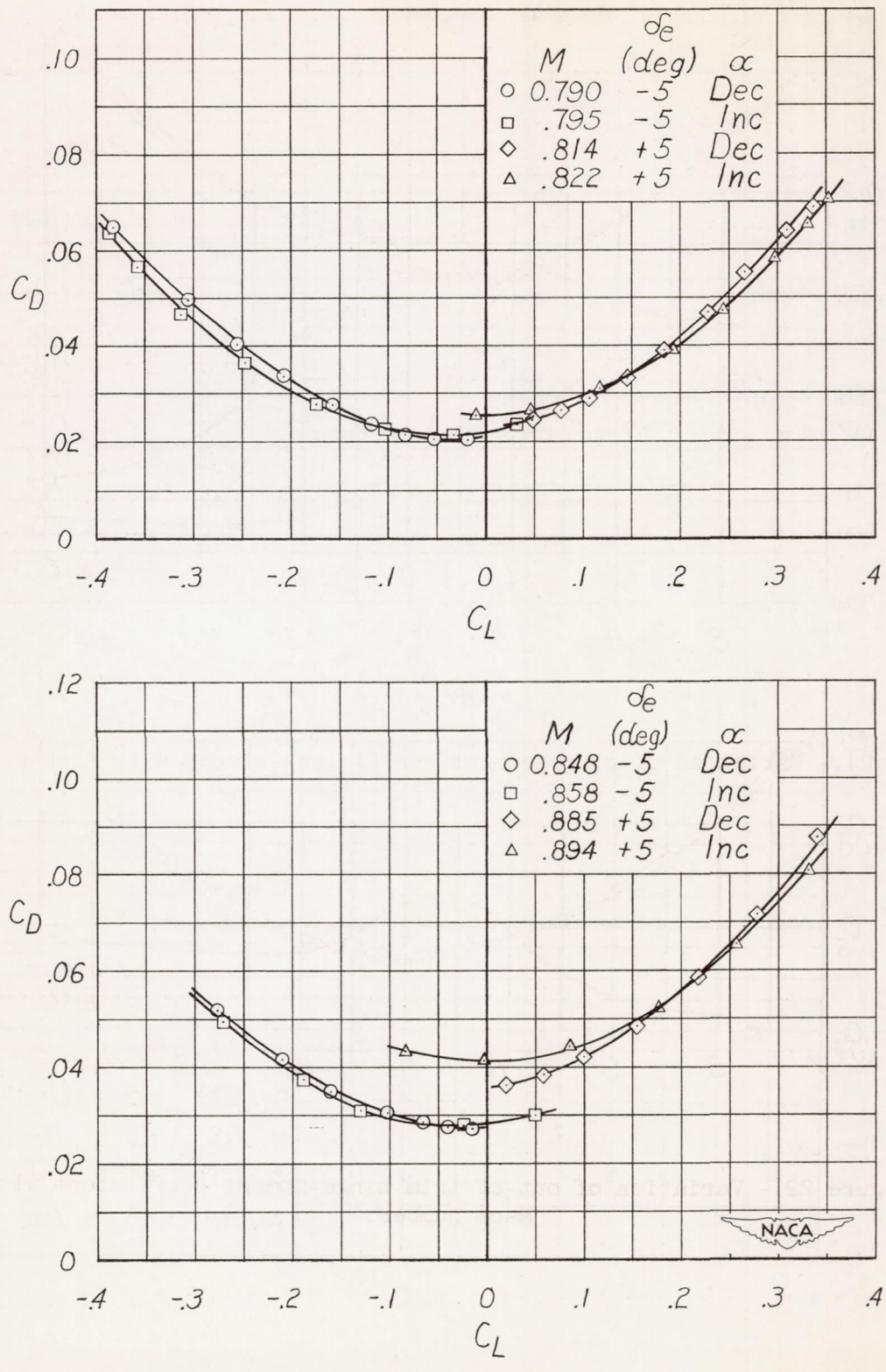

Figure 23.- Lift-drag polar.

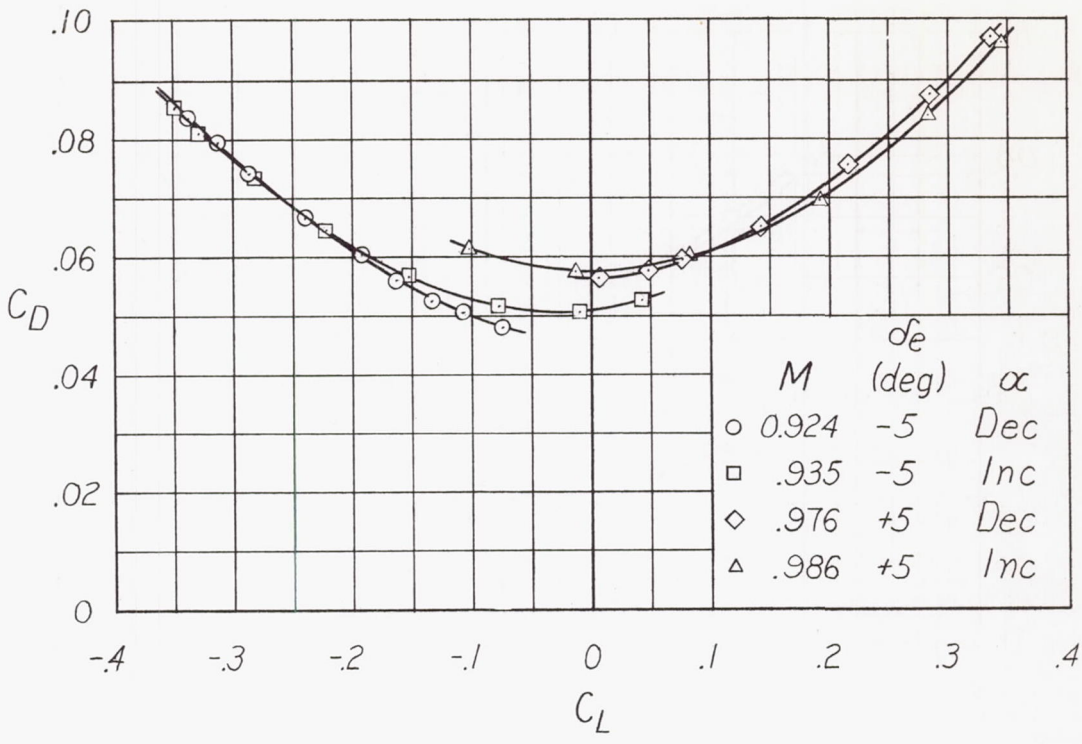

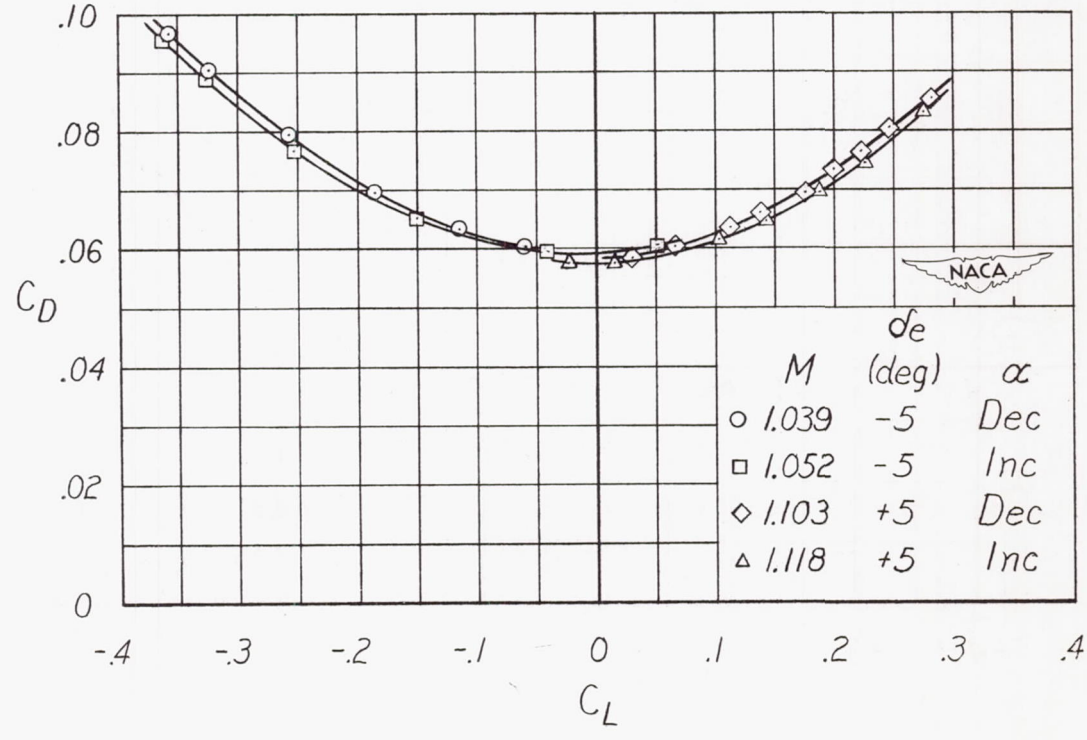

Figure 23.- Continued.

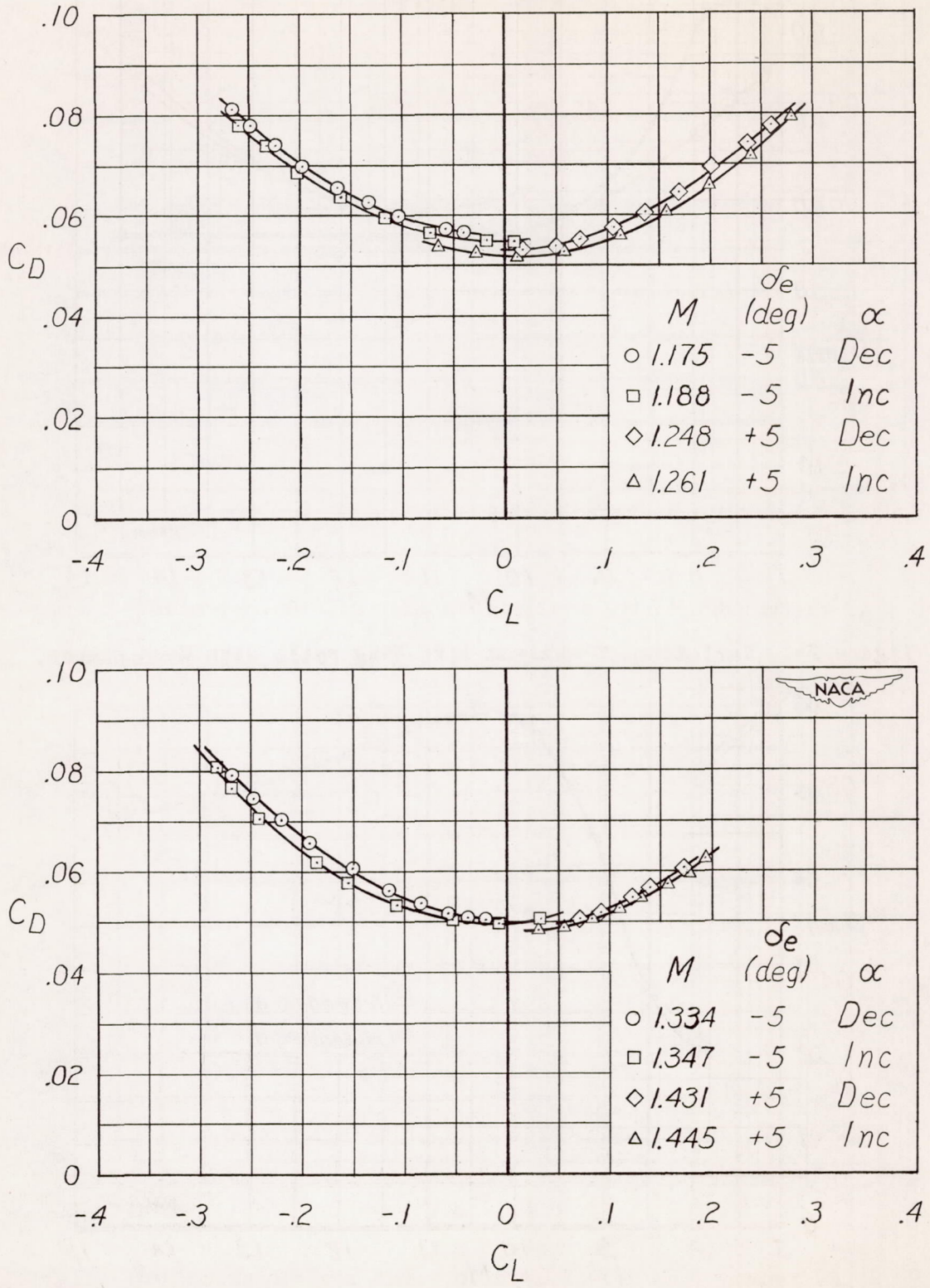

Figure 23.- Concluded.

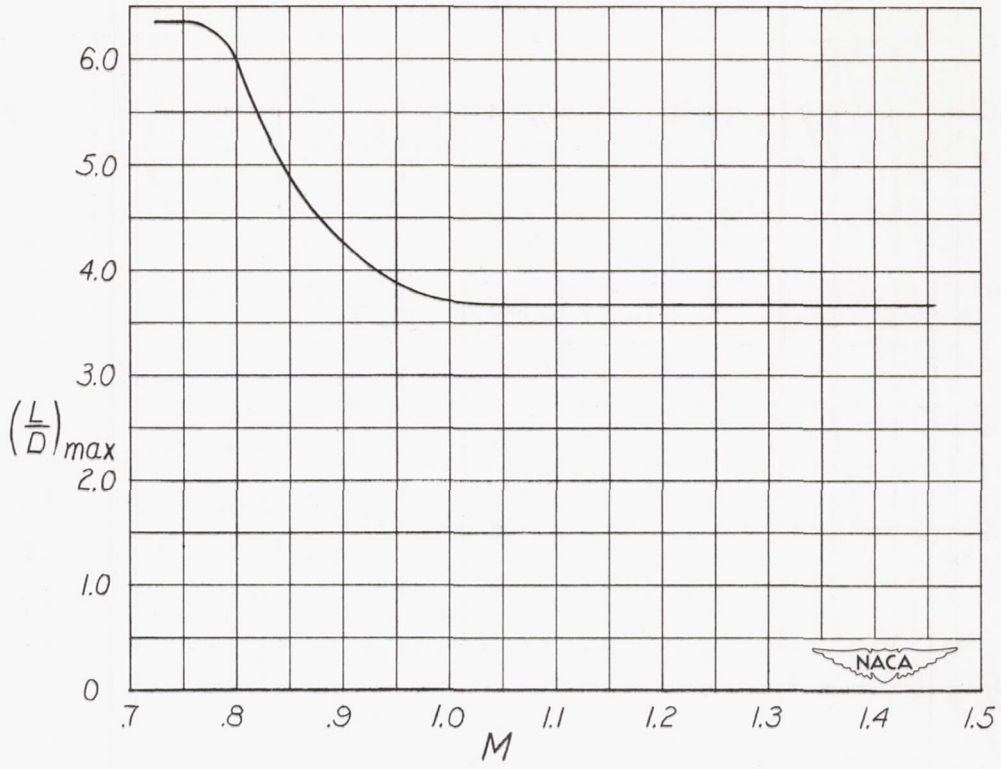

Figure 24.- Variation of maximum lift-drag ratio with Mach number.

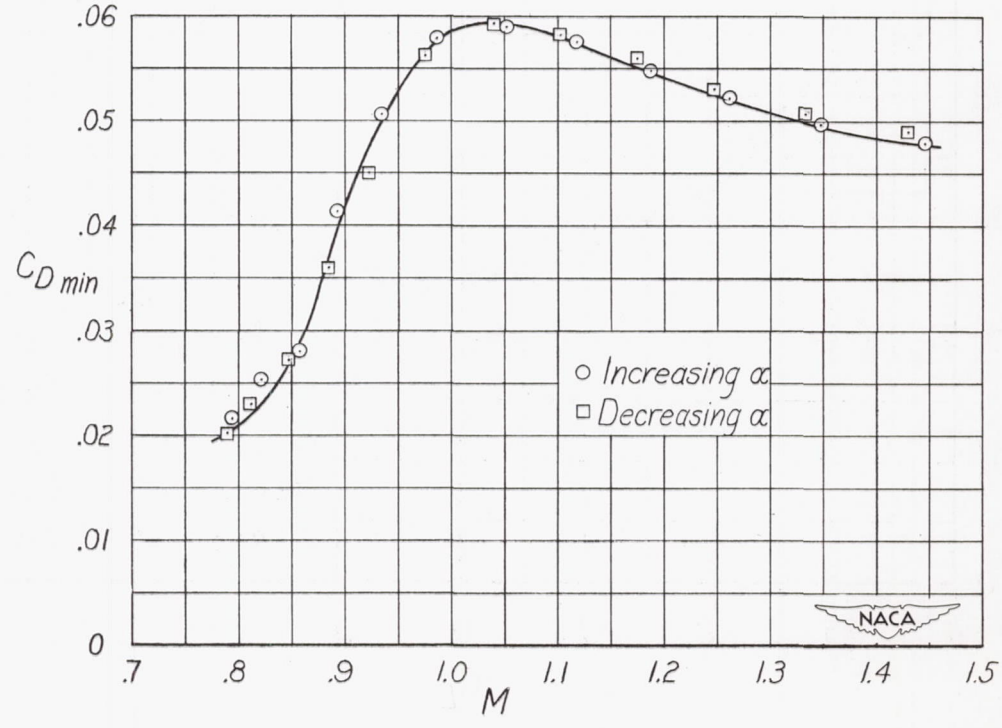

Figure 25.- Variation of minimum drag coefficient with Mach number.

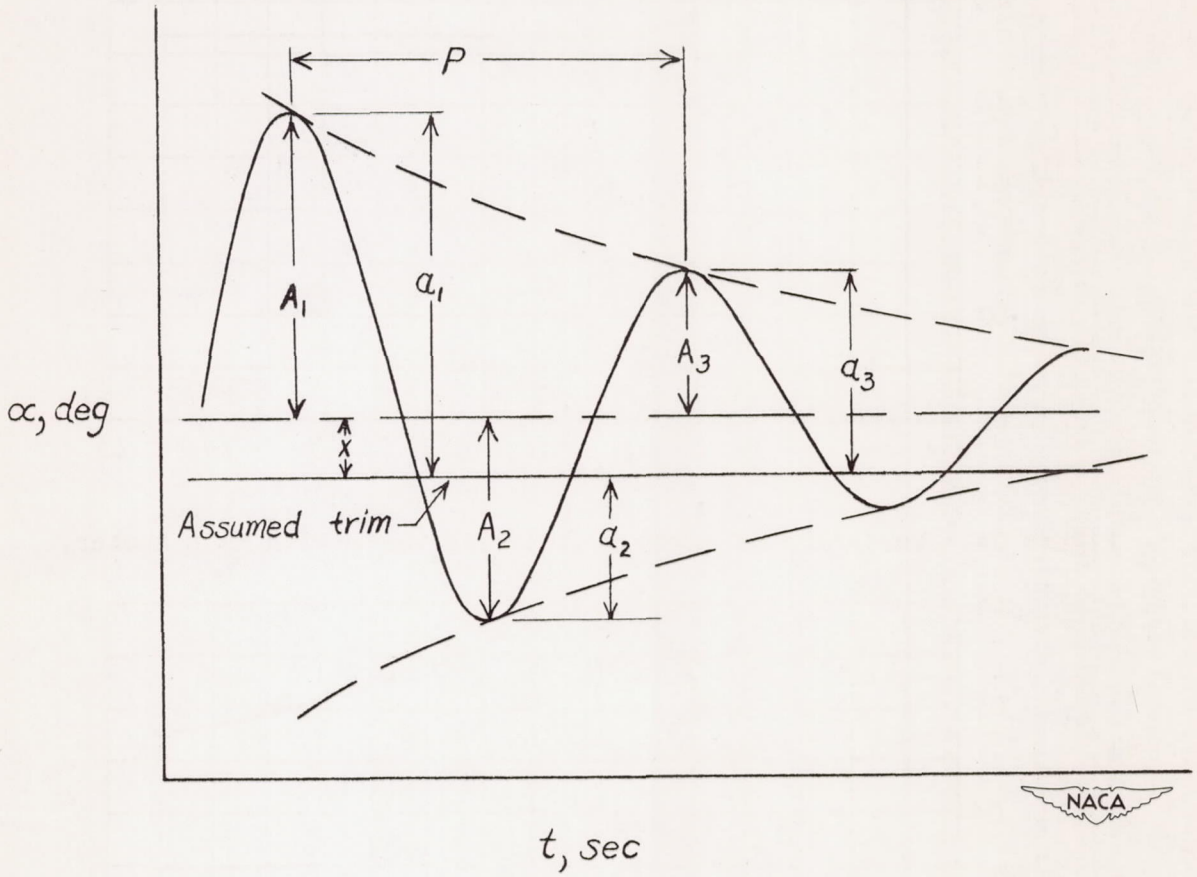

Figure 26.- Angle-of-attack response to step control input.